CHARACTERIZING THE ROLE OF BMI1 IN HUMAN BRAIN TUMOUR INITIATING CELLS

CHARACTERIZING THE ROLE OF BMI1 IN HUMAN BRAIN TUMOUR INITIATING CELLS

By

ERIN L. O`FARRELL, Hon.B.Sc.

A Thesis Submitted to the School of Graduate Studies

in Partial Fulfilment of the Requirements for the Degree

Master of Science

McMaster University MASTER OF SCIENCE (2011) Hamilton, Ontario (Psychology, Neuroscience, & Behaviour)

TITLE: Characterizing the Role of Bmi1 in Human Brain Tumour Initiating Cells

AUTHOR: Erin L. O`Farrell, Hon.B.Sc. (Carleton University)

SUPERVISOR: Dr. Sheila K. Singh

NUMBER OF PAGES: xiv, 102

Abstract

Bmi1 is a member of the Polycomb Group proteins and has been demonstrated as being vital in stem cell regulation. Bmi1 is overexpressed in many cancers, including glioblastoma, and has been shown to regulate cancer cell self-renewal and proliferation both *in vitro* and *in vivo*. This study aimed to determine if Bmi1 modulates brain tumour initiating cell properties using a spontaneous primary glioblastoma cell line and a commercial glioblastoma cell line. To determine the role of Bmi1 in glioblastoma cells, stem cell assays and *in vivo* analysis of tumour formation was performed on both control cells and Bmi1 knockdown cells. In both cell lines, Bmi1 was found to play a positive regulatory role in stem cell properties. When Bmi1 was knocked down in brain tumour initiating cells, properties such as self-renewal, proliferation and tumour formation were impaired compared to control cells. This study supports recent literature which shows that Bmi1 regulates stem cell properties in glioblastoma cells and supports the potential use of Bmi1 as a therapeutic target in glioblastoma brain tumours.

Acknowledgements

This thesis would not have been possible without the help and support of many people. Firstly, I would like to give sincere thanks to my supervisor, Dr. Sheila Singh. Her support and constant guidance helped shape this thesis and advance my scientific skills. To her, I owe the greatest gratitude for her constant encouragement and positivity through all the challenges we encountered along the way.

I would also like to thank all members of my advisory committee, Dr. André Bédard, Dr. Bradley Doble, and Dr. Ray Truant, for all of their guidance and advice throughout the past two years.

Sincere gratitude must be given to all members of the Singh Lab. Without their support and help, this thesis would never have been possible. To Dr. Chitra Venugopal for her lentiviral help and guidance throughout this entire project and to Nicole McFarlane for all flow cytometric work, I could not have achieved anything without you. I would also like to thank Monika Lenkiewicz for all of her teachings and guidance during my first year and Sara Nolte for her support and friendship throughout the past two years.

Finally, the past two years and the completion of this thesis would never been possible without the continuous love and support of my family and friends. The words “thank you” do not adequately express my deep gratitude to you all.

TABLE OF CONTENTS

List of Figures

List of Tables

List of Abbreviations

AML	Acute myeloid leukemia
ARF	Alternative Reading Frame
bFGF	basic fibroblast growth factor
Bmi1	B cell-specific Moloney murine leukemia virus insertion site-1
BTIC	Brain tumour initiating cell
CDK4	Cyclin-dependent kinase 4
CDKN2A	Cyclin-dependent kinase inhibitor 2A
ChIP-Seq	Chromatin immunoprecipitation sequencing
CSC	Cancer stem cell
DMEM	Dulbecco's Modified Eagle Medium
EDTA	Ethylenediaminetetraacetic acid
EGF	Epidermal growth factor
EGFR	Epidermal growth factor receptor
FBS	Fetal bovine serum
GAPDH	Glyceraldehyde 3-phosphate dehydrogenase
GBM	Glioblastoma
GFAP	Glial fibrillary acidic protein
GFP	Green fluorescent protein
HLA	Human leukocyte antigen
hTERT	human telomerase reverse transcriptase
Id1	Inhibitor of differentiation and DNA binding 1
IDH1/IDH2	Isocitrate dehydrogenase 1 or 2
INK4A	Inhibitor of cyclin-dependent kinase 4

LIF	Leukemia inhibitory factor
MAP2	Microtubule-associated protein 2
mir128	microRNA 128
MOI	Multiplicity of infection
mRNA	Messenger ribonucleic acid
NF1	Neurofibromin 1
NOD-SCID	Non-obese diabetic severe combined immunodeficient
NSC	Neural stem cell
NSG	NOD/SCID gamma immunodeficient
PBS	Phosphate buffered saline
PcG	Polycomb group
PDGFRα	Platelet-derived growth factor receptor alpha
PI3K	Phosphoinositide 3-kinase
PIP2	Phosphatidylinositol 4,5-bisphosphate
PIP3	Phosphatidylinositol (3,4,5)-trisphosphate
PTEN	Phosphatase and tensin homolog
PRC	Polycomb repression complex
Rb	Retinoblastoma protein
shBmi1	short hairpin RNA targeting Bmi1
Shh	Sonic hedgehog
shLuc	short hairpin RNA targeting Luciferase
shRNA	short hairpin RNA
TIC	Tumour initiating cell

Declaration of Academic Achievement

The completion of this thesis was the result of contributions from all Singh lab members and myself. In particular, Dr. Chitra Venugopal performed all lentiviral work, RT-PCR, and Western Blot analysis. Nicole McFarlane performed all flow analysis and cell sorting. Sara Nolte assisted with BT 241 flow analysis and secondary sphere formation assays. For *in vivo* work, assistance was provided by Dr. Chitra Venugopal, Sara Nolte, and Branavan Manoranjan. Pathological analysis of *in vivo* tumours was provided by Dr. Jacek Kwiecien.

Chapter 1.

INTRODUCTION

1.1 Glioblastoma

Malignant gliomas are the most common primary brain tumour in adults, representing 70% of primary brain tumours (Wen & Kesari, 2008). The most prevalent and aggressive type of malignant glioma is termed glioblastoma (GBM) (Holland, 2000; Huse & Holland, 2010; Oliver & Wechsler-Reya, 2004). Glioblastomas arise from glial cells within the central nervous system and are extremely heterogeneous tumours displaying both intertumoural as well as intratumoural heterogeneity (Bonavia *et al*., 2011; Holland, 2000; Chen *et al*., 2011; Wen & Kesari, 2008). The heterogeneity of GBM extends to every level of the tumour from gross morphology down to genetic mutations (Holland, 2000). Pathologically, glioblastomas are characterized by high levels of proliferation, nuclear atypia, endothelial hypertrophy and hyperplasia, and necrosis (Huse & Holland, 2010; Miller & Perry, 2007). At the molecular level, glioblastomas are characterized by a multitude of mutations which can include *p53* mutations, amplification of the epidermal growth factor receptor (*EGFR*), loss of chromosome 1p and 19q, amplification of cyclin-dependent kinase 4 (*CDK4*), deletion of cyclin-dependent kinase inhibitor 2A (*CDKN2A*), deletion of retinoblastoma protein (Rb), amplification of platelet-derived growth factor receptor-α (*PDGFRα*), loss of phosphatase and tensin homolog (*PTEN*), deletion of neurofibromin 1 (*NF1*), or a mutation in isocitrate dehydrogenase 1 or 2 (*IDH1*/*IDH2*) (Huse & Holland, 2010; Verhaak *et al*., 2010; Wen & Kesari, 2008).

Glioblastomas are diffuse in nature, with tumorigenic cells invading vital areas of the brain, leaving no focal tumour to target with current therapies, and resulting in an inevitably poor prognosis (Holland, 2000). Treatment for these tumours, which has not changed significantly for several decades, involves surgical resection of the bulk tumour followed by radiation and chemotherapy to target the diffusely invading cells. Average life expectancy for patients, even

with aggressive treatment, is 12 to 15 months (Holland, 2000; Huse & Holland, 2010; Oliver & Wechsler-Reya, 2004; Wen & Kesari, 2008).

1.2 Cancer Stem Cell Hypothesis

The idea that cancer cells arise from stem-like cells is not a new one. In 1867, the German scientist Cohnheim suggested that cancer was the result of abnormal embryonic cells, now known to be stem cells, or cells with stem cell properties (Tan *et al*., 2006). Stem cells make an appealing "cell of origin" as they possess the capacity for self-renewal, providing long life spans with time to acquire multiple mutations and become cancerous (Reya *et al*., 2001; Wicha *et al*, 2006).

The idea that a rare sub-population of cells within both circulating cancers and solid tumours have the ability to self-renew and proliferate *in vitro*, as well as reconstitute the original tumour phenotype *in vivo*, defines the cancer stem cell hypothesis. This hypothesis states that there is a hierarchy of cancer cells ranging from "stem-like" cells, termed tumour initiating cells (TICs), which have high proliferative capacity allowing the expansion of a tumour, down to more differentiated cells which possess restricted proliferative capacity (Clarke *et al*., 2006; Dalerba *et al*., 2007; Ishizawa *et al*., 2010; O'Brien *et al*., 2009; Pardal *et al*., 2003; Shackleton *et al*., 2009; Shipitsin & Polyak, 2008; Visvader & Lindeman, 2008; Wicha *et al*., 2008). Cancer stem cells are thought to either be derived from normal stem cells or from more committed progenitor cells which have acquired the ability to self-renew and maintain tumour growth through mutations (Ailles & Weissman, 2007; Clarke *et al*., 2006). The cancer stem cell hypothesis is an alternative hypothesis to the clonal evolution model which suggests that, within a tumour, all cells have an equal capacity to generate and maintain tumour growth. Within this hypothesis, certain cells

have a growth advantage and as a result, are selected for throughout tumour development (O'Brien *et al*., 2009; Reya *et al*., 2001; Shackleton *et al*., 2009; Vescovi *et al*., 2006; Visvader & Lindeman, 2008; Wicha *et al*, 2006). The cancer stem cell hypothesis states that cancer stem cells are similar to somatic, or adult, stem cells with several key differences. Although somatic stem cells and cancer stem cells share many properties, such as the ability to self-renew and differentiate into multiple lineages, one key difference between these two cells types is their ability to regulate these stem cell properties. While somatic stem cells self-renew and differentiate in an extremely controlled manner, cancer stem cells do so in an uncontrolled and abnormal fashion (Pardal *et al*., 2003). Another distinction between somatic stem cells and cancer stem cells must also be made clear: although both cell types show extensive self-renewal and proliferation, cancer stem cells are defined by their ability to initiate and maintain tumour formation *in vivo* (Clarke *et al*., 2006; Oliver & Wechsler-Reya, 2004; Vescovi *et al*., 2006). The idea of cancer stem cells is an appealing one from a clinical standpoint as these cells make excellent candidates for therapy evasion. Normal neural stem cells have been shown to possess drug resistance abilities through the use of efflux pumps as well as DNA repair mechanisms. If cancer stem cells are similar to normal stem cells, they too would possess these evasion properties, supporting the hypothesis that a subpopulation of cells can evade cancer therapy and regenerate the tumour in patients (Ailles & Weissman, 2007). This evasion of therapy has been demonstrated in acute myeloid leukemia (AML) cancer stem cells which possess drug efflux pumps as well as $CD133^{+}$ cancer stem cells which possess increased DNA damage repair activity (Steinbach & Legrand, 2007; Bao *et al*., 2006).

Cancer stem cells were first identified in AML through the use of cell surface markers $CD34^{+}CD38^{-}$ which were used to isolate a highly proliferative "stem cell" population from the

AML cell population (Bonnet & Dick, 1997). These cells both possessed high self-renewal and were capable of initiating AML in immunocompromised mice which recapitulated the original patient AML phenotype (Bonnet & Dick, 1997). This original identification of cancer stem cells ruled out the stochastic model of tumour heterogeneity for leukemia. Following this discovery, the first solid tumour cancer stem cells were discovered in breast cancer using the surface markers $CD44^{+}CD24^{-}$ (Al-Hajj *et al*., 2003) and shortly thereafter in medulloblastoma and glioblastoma using the surface marker $CD133^{+}$ (Singh *et al*., 2003; Singh *et al*., 2004b). These subpopulations of cells all demonstrated high self-renewal and multipotentiality both *in vitro* and *in vivo* as compared to their non-cancer stem cell counterparts (Al-Hajj *et al*., 2003; Singh *et al*., 2003; Singh *et al*., 2004b).

1.3 Brain Tumour Initiating Cells

Brain tumours are composed of both neurons and glial cells which suggest that they may also contain pluripotent progenitor cells. Brain tumours have also been demonstrated as expressing neural stem/progenitor cell markers such as CD133 and nestin (Oliver & Wechsler-Reya, 2004). Primary brain tumour cells, isolated from patient samples, cultured *in vitro* form neurospheres, or "tumour spheres", under serum-free culture conditions similarly to neural stem cells (Singh *et al*, 2003). When placed under differentiation conditions, these tumour cells differentiate into both neurons and glial cells which reflect the heterogeneity of the primary tumour. These observations *in vitro* indicate that brain tumour cells have the capacity for self-renewal and multi-lineage differentiation similar to neural stem cells (Oliver & Wechsler-Reya, 2004; Singh *et al*., 2003). This observation of neural stem-like cells in brain tumours suggests that a subset of tumour cells can be classified as "cancer stem cells" (Oliver & Wechsler-Reya, 2004, Singh *et al*, 2003).

Brain tumour initiating cells (BTICs) were originally identified when a subpopulation of primary brain tumour cells in non-adherent cell culture conditions selecting for neural stem cell growth formed tumour spheres within 48 hours of placing these cells into culture (Singh *et al*., 2003). Over time, these tumour spheres continued to thrive and proliferate, while the other cells within the culture either adhered and differentiated or simply lost the ability to proliferate. The isolated tumour spheres were then analysed for marker determination and found to be nestin positive and CD133 positive. Nestin is an intermediate filament protein which is used as a neural stem cell marker as it is found in undifferentiated neural cells. CD133 is a five transmembrane protein of unknown biological function originally used to identify hematopoietic stem and progenitor cells and thought to be a neural stem cell marker as it has been used to isolate fetal human neural stem cells (Tabatabai & Weller, 2011; Singh *et al*., 2003; Singh *et al*.,2004a; Uchida *et al*., 2000; Yin *et al*., 1997). The tumour spheres were subjected to neural stem cell assays to determine self-renewal, proliferative, and differentiation capacity. Interestingly, when $CD133^+$ cells and $CD133^-$ cells were isolated and cultured independently, $CD133^+$ cells showed the proliferative characteristics of whole tumour spheres while $CD133^-$ cells exhibited adherence and a decrease in proliferation. As well as displaying stem cell-like properties, the isolated $CD133^+$ cells, when differentiated, displayed an identical phenotype to the original primary tumour rather than differentiating as normal neural stem cells into 20-30% neurons, 50-60% astrocytes, and 5-10% oligodendrocytes. This observation indicated that the isolated subpopulation of cells were not normal neural stem cells but rather tumour cells with stem cell-like properties (Singh *et al*., 2003). Further *in vivo* characterization of this subpopulation of cells revealed that only the $CD133^+$ population were capable of forming tumours in non-obese diabetic severe combined immunodeficient (NOD-SCID) mice. In fact, an injection of 100,000 $CD133^-$ cells did not

initiate tumour formation whereas an injection of 100 $CD133^+$ cells was able to initiate tumour formation (Singh *et al*., 2004b). The xenograft tumours also recapitulated the original patient tumour phenotype. To truly confirm whether these $CD133^+$ cells reflected a cancer stem cell population, serial re-transplantation of primary xenografts was performed. All mice injected serially with primary xenograft cells exhibited tumour formation and the secondary tumour reflected the original patient tumour phenotype confirming that the $CD133^+$ subpopulation of cells displayed *in vivo* self-renewal and reflected a cancer stem cell population (Singh *et al*., 2004b).

1.4 Caveats of the Cancer Stem Cell Hypothesis

Much debate exists around the ideas proposed in the Cancer Stem Cell Hypothesis. The main argument against the Cancer Stem Cell Hypothesis is that the hypothesis attributes cancer properties to the intrinsic cellular processes and may not account for extrinsic factors such as environmental niche and immune system (Rosen & Jordan, 2009). Normal stem cells require a niche for survival and maintenance of stem cell properties, therefore the same must hold true for cancer stem cells, however, this has not yet been fully explored within the Cancer Stem Cell Hypothesis (Shipitsin & Polyak, 2008). This argument is further supported by the idea that the "gold standard" for demonstrating the existence of cancer stem cells is serial re-transplantation in a xenograft model. Xenografts, although informative, do not provide human cells with the appropriate extrinsic factors and cues. In this regard, it is argued that xenograft models merely select for cells which are better able to survive in a mouse environment rather than selecting for truly tumorigenic cells (Clarke *et al*., 2006; Hadjipanayis & Van Meir, 2009; Kelly *et al*., 2007; Marquardt *et al*., 2010; Rosen & Jordan, 2009; Shipitsin & Polyak, 2008, Visvader & Lindeman, 2008). This is especially true for solid tumours which require extensive niches for growth,

including endothelial cells and extensive vasculature (Shipitsin & Polyak, 2008). The niche of a tumour is so important that it has even been shown that the site of injection of tumour cells can create marked differences in engraftment rates and therefore cancer stem cell read-out (Clarke *et al*., 2006; Visvader & Lindeman, 2008). This has been demonstrated using GBM cells which, when injected subcutaneously, resulted in a 50% engraftment rate as compared to 100% engraftment when injected intracranially (Galli *et al*., 2004). Furthermore, intrinsic factors of cancer cells such as genomic instability and rapid changes in marker expression are not accounted for by the Cancer Stem Cell Hypothesis. Malignant cells are known to change over time and adapt to environmental changes, thus raising the question about the validity of using surface markers to isolate so-called cancer stem cells. Not only have surface markers been shown to be stochastically activated by culture conditions thus impacting the true isolation of a cancer stem cell, the ever changing nature of malignant cells dictates that surface marker expression would change rapidly as a result of environmental changes and stressors (Clarke *et al*., 2006; Emmenegger & Wechsler-Reya, 2008; Marquardt *et al*., 2010; Shipitsin & Polyak, 2008). As well as surface marker expression changes as a result of environment, technical issues such as different cell preparation techniques and different isolation techniques leads to marked differences in supposed cancer stem cell frequencies as reported by different groups (Clarke *et al*., 2006; Visvader & Lindeman, 2008).

1.5 Bmi1

The *Bmi1* (B cell-specific Moloney murine leukemia virus insertion site-1) gene is located on the plus strand of chromosome 10 at 22,605,381 bp from *pter* (Alkema *et al.*, 1993). The gene extends over a 4.9Kb range and comprises 10 exons and 9 introns (Jiang *et al*., 2009). The functional promoter region of *Bmi1* has yet to be conclusively defined and as a result, most

researchers use a sequence of 20-30 base pairs upstream of the translational start site as the promoter (Abdouh *et al*., 2009; Alkema *et al*., 1993; Chiba *et al*., 2008; Zencak *et al*., 2005). The Bmi1 protein is 37KDa and is comprised of 326 amino acids. It is mainly found in the nucleus but is also present in the cytoplasm of a cell (Cohen *et al*., 1996). Bmi1 contains a RING-type zinc finger at the N-terminus of the protein and a conserved helix-turn-helix site in its centre (Alkema *et al*., 1993; Dimri *et al*., 2002; Jiang *et al*., 2009; Park *et al*., 2004).

Bmi1 is a member of the highly conserved polycomb group (PcG) genes and acts as a transcriptional repressor of multiple genes, including genes which determine proliferation and differentiation of cells throughout development (Alkema *et al*., 1993; Bracken *et al*., 2010; Chen *et al*., 2010; Sauvageau & Sauvageau, 2010; Schuringa & Vellenga, 2010; Valk-Lingbeek *et al*., 2004). Bmi1 is one of several subunits in the polycomb repression complex 1 (PRC1) which is also comprised of Mel-18, Ring1A/B, CBX2, CBX4, CBX6, CBX7, CBX8, and PH1/PH2 (Li *et al*., 2006). A second repression complex, PRC2, is comprised of the subunits EZH2, EED, SUZ12, and RbAp46/48. Together PRC1 and PRC2 are responsible for the transcriptional regulation of multiple genes through histone modifications (Bracken *et al*., 2010; Kallin *et al*., 2009; Schuringa & Vellenga, 2010). The initial step of transcriptional regulation involves the trimethylation of histone 3 on lysine 27 by PRC2 which compacts the chromatin. The catalytically active subunit of PRC2 responsible for this step is EZH2, a histone methyltransferase specific to lysine 27 of histone 3 and lysine 26 of histone 1. The PRC1 subunits recognize the H3K27 trimethylation mark (H3K27me3) left by PRC2 and subsequently induce the monoubiquitination of lysine 119 of histone H2A. The monoubiquitination of lysine 119 of histone H2A is made possible by Bmi1 which binds to Ring1B thus stimulating its E3 ligase activity (Bracken *et al*., 2006; Bracken *et al*., 2010; Kallin *et al*., 2009; Li *et al*., 2006;

Schuringa & Vellenga, 2010; Wang *et al*., 2004). The monoubiquitination of H2A then represses gene transcription or induces complete silencing by physically blocking RNA Polymerase II (Bracken *et al*., 2010; Schuringa & Vellenga, 2010; Zhou *et al*., 2008).

The monoubiquitination of H2A leaves a uH2A mark which can be detected using chromatin immunoprecipitation sequencing (ChIP-Seq) technology. Using this technology, it was found that Bmi1-dependent uH2A marks are increased at genes which are silenced or have low expression, confirming that Bmi1 represses such genes (Kallin *et al*., 2009). It was also found that there was a bias of Bmi1-dependent uH2A marks present at genes which contained H3K27me3 marks, however, some uH2A marks were still present where no H3K27me4 marks existed, indicating that there may be other unknown recruitment mechanisms for PRC1 other than PRC2 (Kallin *et al*., 2009).

Interestingly, PcG binding and H3K27me3 marks are found to be increased within stem cells and are associated with self-renewal. During differentiation, binding decreases and repression is released, allowing the transcription of certain genes. It is also thought that the increased PcG binding seen in stem cells may be associated with certain cancer causing mutations, such as overexpression of oncogenes like *Bmi1* or silencing of tumour suppressor genes (Bracken *et al*., 2006).

1.6 Bmi1 and Cancer

Within normal neural stem cells, Bmi1 has been shown to play a role in self-renewal and proliferation. Bmi1 overexpression has been demonstrated as resulting in increased self-renewal and proliferation as well as decreased differentiation, thus making it an excellent target for potential deregulation within cancer (He *et al*., 2009; Yadirgi *et al*., 2011). *Bmi1* was first

identified as an oncogene which cooperated with the oncogene *c-myc* within murine lymphomagenesis (Haupt *et al*., 1991; van Lohuizen *et al*., 1991). Bmi1 has since been demonstrated as being present and often overexpressed in multiple cancers including leukemia, hepatocellular carcinoma, laryngeal carcinoma, lung cancer, breast cancer, colon cancer, and brain tumours such as medulloblastoma and glioblastoma (Schuringa & Vellenga, 2010; Chiba *et al*., 2008; Chen *et al*., 2010; Silva *et al*., 2006; Kim *et al*., 2004; Leung *et al*., 2004; Abdouh *et al*., 2009; He *et al*., 2009; Jacobs *et al*., 1999a; Liu *et al*., 2006). Interestingly, within glioblastoma cells, overexpression of Bmi1 is not associated with gene amplification therefore it is most likely the result of increased transcription (Abdouh *et al*., 2009).

One of the most studied Bmi1 pathways associated with cancer is the repression of the *INK4A/ARF* locus. The *INK4A/ARF* locus is located on chromosome 9p21, a chromosome whose short arm is often mutated in human cancers (Sharpless & DePinho, 1999). Within this pathway, Bmi1 directly or indirectly represses transcription of CDKN2A, which encodes for the two cyclin dependent kinases INK4A and ARF (Abdouh *et al*., 2009; Gil *et al*., 2005; Pardal *et al*., 2003). It has been demonstrated that increased Bmi1 levels are associated with low INK4A and ARF levels indicating a potential regulatory role by Bmi1 (Kim *et al*., 2004).

The inhibitor of cyclin-dependent kinase 4 (INK4A) family of proteins contains the tumour suppressor p16 which acts in the retinoblastoma protein (pRB) cellular growth pathway. Within this pathway, p16 binds to and inhibits CDK4/cyclin D by inhibiting its kinase activity through the distortion of the cyclin-binding site. This prevents ATP binding and subsequently prevents the phosphorylation of pRB (Grinstein & Wernet, 2007; Ivanchuk *et al*., 2001; Sharpless & DePinho, 1999). This causes an arrest in the cell-cycle progression and senescence in cells. Interestingly, pRB is essential to this cell cycle arrest, as seen in cells lacking pRB which do not

show arrest even when levels of p16 are increased. Clinically, this is seen in many gliomas which have a loss of *pRB* but retain *p16* (Ivanchuk *et al*., 2001).

The Alternative Reading Frame (*ARF*) locus encodes for the protein p14 (p19 in mice) and acts on the p53-mediated cellular growth pathway. In this pathway, p14 inhibits MDM2, a ubiquitin ligase responsible for targeting p53 for degradation by displacing it from the nucleus to the nucleolus. This leaves p53 free to act as a transcription factor for its downstream targets, resulting in an inhibition of cell cycle progression and the promotion of apoptosis (Grinstein & Wernet, 2007; Ivanchuk *et al*., 2001).

Bmi1 regulates *INK4A* and *ARF* through transcriptional repression in a dose-dependent manner (Jacobs *et al*., 1999b). Through direct or indirect inhibition of *CDKN2A* transcription, Bmi1 inhibits p16 thus preventing the suppression cyclin D dependent kinases and inducing phosphorylation of retinoblastoma protein (Rb) resulting in increased cell proliferation. Bmi1 also acts by suppressing p14/p19, through repression of *CDKN2A* transcription, thus preventing its binding to MDM2. This subsequently allows MDM2 to bind to and degrade p53 resulting in decreased apoptosis (Bruggeman *et al*., 2007; Chen *et al*., 2010; Jacobs *et al*., 1999a; Jacobs *et al*., 1999b; Pardal *et al*., 2003). These findings have been verified consistently in mouse embryonic fibroblasts however, in human embryonic fibroblasts, it has been found that overexpression of Bmi1 decreases *INK4A* transcription but not *ARF* transcription (Bracken *et al*., 2010). Further analysis found that the PRC1 and PRC2 combine and "blanket" the *INK4A* locus, a 10Kb locus, but do not repress *ARF* in the same manner as seen by the H2A mark on *INK4A* promoter but not on the *ARF* promoter (Bracken *et al*., 2010). Importantly, in order for Bmi1 to continuously repress the *INK4A/ARF* locus, PRC2 must be continuously associated. If

components of PRC2, such as EZH2 or SUZ12, are downregulated, Bmi1 dissociates from the promoter and transcription is no longer repressed (Bracken *et al*., 2010).

Many other potential Bmi1 pathways exist which may be involved in cancer progression. One method of repression may involve the oncogene *c-myc*, a member of a family of transcription factors important for cell proliferation and differentiation throughout development. Overexpression of c-myc has been linked to tumorigenesis through decreased differentiation and increased self-renewal however when expressed alone, it induces mouse embryonic fibroblast apoptosis through increased p19 transcription (Jacobs *et al*., 1999b; Li *et al*., 2009). When Bmi1 and c-myc are expressed together, however, apoptosis is prevented and proliferation is increased. When *INK4A/ARF* is lost, this relationship is not seen, thus it has been speculated that Bmi1 inhibits apoptosis by c-myc through direct inhibition of the *INK4A/ARF* locus, which results in increased proliferation and transformation (Alkema *et al*., 1993; Jacobs *et al*., 1999b).

Another pathway of repression involves human telomerase reverse transcriptase (hTERT) which activates telomerase activity, preventing telomere erosion and cellular senescence. It has been found that Bmi1 may bind to and activate transcription of hTERT, leading to the immortalization of mammary epithelial cells through telomerase activity; however, this binding appears to be cell-type specific, as this effect was not seen in human fibroblasts (Dimri *et al*., 2002).

Another Bmi1 pathway of repression involves the helix-loop-helix inhibitor of differentiation and DNA binding (*Id1*). *Id1* is a well known oncogene which stimulates cell cycle progression and cell proliferation. *Id1* activates the serine/threonine protein kinase, Akt, pathway and leads to increased phosphorylation of Akt. The increased phosphorylation of Akt induces the degradation of Mel-18, a subunit of the PRC1 complex, which leads to the activation of c-myc. C-myc then

binds to the E-box in the *Bmi1* promoter inducing transcription of Bmi1 in the nucleus. Bmi1 then binds to RING1B and increases its E3 ligase activity subsequently promoting histone H2A ubiquitination at lysine 119 which leads to the silencing of genes such as *p14* and *p16* (Qian *et al*., 2010).

Together, these pathways reveal several potential targets of Bmi1 mutation which could result in uncontrolled proliferation and cancer.

1.7 Bmi1 Knockdown

Bmi1 has been found to be essential for the self-renewal and proliferation of both normal neural and hematopoietic stem cells (Abdouh *et al*., 2009; Ailles & Weissman, 2007; Bruggeman *et al*., 2007; Chen *et al*., 2010; Fasano *et al*., 2007; Gil *et al*., 2005; Lessard & Sauvageau, 2003; Park *et al*., 2004). It has been demonstrated as a key component of PRC1, as the loss of Ring1a or M33 from the complex do not affect self-renewal of neurospheres, while loss of Bmi1 causes clear deficits in self-renewal (Bruggeman *et al*., 2005). Bmi1 deficiency has been demonstrated as having a negative effect on self-renewal, proliferation, and differentiation potential in multiple cell types including normal murine neural stem cells, hematopoietic stem cells and cancer stem cells both *in vitro* and *in vivo* (Fasano *et al*., 2009; Molofsky *et al*., 2003; Bruggeman *et al*., 2007; Iwama *et al*., 2004; Schuringa & Vellenga, 2010; Abdouh *et al*., 2009; Chen *et al*., 2010; Gil *et al*., 2005; Lessard & Sauvageau, 2003).

Within mouse embryonic fibroblasts, Bmi1 deficiency leads to premature senescence of cells as compared to wild-type fibroblasts, while overexpression of Bmi1 immortalizes fibroblasts through increased cell proliferation (Jacobs *et al*., 1999a). Decreased cell growth and increased apoptosis is also seen when Bmi1 is knocked down in normal cells and normal stem cells,

however the effect is much more acute (Liu *et al*., 2006). Interestingly, some researchers have found that when Bmi1 is knocked down in neural stem cells, self-renewal and proliferation decrease, however survival and differentiation of cells remains similar between control cells and *Bmi1*$^{-/-}$ cells (Molofsky *et al*., 2003).

Bmi1 has been demonstrated as being crucial for self-renewal and proliferation both *in vitro* as well as *in vivo*. In fact, *in vivo* analyses of GBM cells showed increased caspase-3 activity 10 days post-injection in Bmi1 knockdown cells, indicating increased apoptosis and suggesting that Bmi1 is necessary for tumour formation *in vivo* (Abdouh *et al*., 2009). Also, *in vitro* studies of GBM cells indicated that when Bmi1 is knocked down, levels of human leukocyte antigen (HLA) immune response molecules increase, suggesting that Bmi1 may support tumour evasion from host immune cells through inhibition of HLA molecules (Abdouh *et al*., 2009).

When Bmi1 is knocked down in both haematopoietic stem cells and cancer stem cells, levels of p14 and p16 become upregulated and reactive oxygen species levels increase, resulting in decreased cell growth and increased apoptosis (Bruggeman *et al*., 2007; Gil *et al*., 2005; Jacobs *et al*., 1999a; Liu *et al*., 2006; Molofsky *et al*., 2003; Schuringa & Vellenga, 2010). Further studies have indicated that Bmi1 knockdown in GBM cells inhibits cell proliferation and self-renewal *in vitro* through increased apoptosis and differentiation, independent of a functional *INK4A/ARF* locus, suggesting alternative pathways for Bmi1 repression (Abdouh *et al*., 2009). When studied further using microarray and ChIP analysis on *INK4A/ARF* -/- GBM tumours, it was determined that in the absence of *INK4A/ARF*, Bmi1 binds to and inhibits *p21*, which blocks cell growth through the inhibition of CDK4 and prevention of Rb phosphorylation and maintains the Rb-E2F complex required to repress cell-cycle progression (Abdouh *et al*., 2009; Fasano *et al*., 2007). Bmi1 inhibition on *p21* has also been demonstrated in normal murine neural stem

cells in which Bmi1 knockdown revealed an increase in *p21* levels but no change in *p16* or *p19* levels (Fasano *et al*., 2007). Furthermore, *p18* was found to be increased in *INK4A/ARF* -/- GBM tumours and increased further when Bmi1 was knocked down leading investigators to believe that *p18* compensated for *p16* deletion in gliomas and was a target of Bmi1 suppression (Abdouh *et al*., 2009).

When prostate cancer cells are subjected to Bmi1 knockdown, levels of *p53* and *PTEN* increase, while levels of cyclin D1 decrease. Of particular interest is phosphatase and tensin homolog (PTEN), a tumour suppressor which dephosphorylates phosphatidylinositol (3,4,5)-trisphosphate (PIP3) into phosphatidylinositol 4,5-bisphosphate (PIP2) thus inhibiting phosphoinositide 3-kinase (PI3K) mediated tumorigenic activity. It has been demonstrated that PTEN binds to and inhibits Bmi1 in the nucleus of prostate cancer cells thus releasing the suppression of p16 and p14 and preventing Bmi1-mediated proliferation (Fan *et al*., 2009; Chen *et al*., 2010; Schuringa & Vellenga, 2010). However, PTEN is often inactivated in glioblastoma tumours perhaps allowing Bmi1 to suppress apoptosis and cell cycle exit (Vescovi *et al*., 2006).

Through siRNA studies, it was found that depletion of any number of PRC1 or PRC2 members led to an increase in the other members of the complexes indicating that Polycomb Group genes autoregulate their synthesis in response to changes in expression of other complex members (Bracken *et al*., 2006). Interestingly, when Bmi1 is knocked down in cells, levels of the PRC1 complex member CBX7 increase and rescue senescence of cells and when CBX7 is knocked down, Bmi1 levels rise and rescue senescence indicating potential autoregulation within the complex and another potential method of mediating proliferation (Gil *et al*., 2005).

Although Bmi1 is implicated in multiple cancer types, its pathway is not yet fully understood (Schuringa & Vellenga, 2010). It is well known that Bmi1 binds to and represses *p14* and *p16* thus leading to decreased apoptosis and increased proliferation respectively, however, the upstream regulators of Bmi1 have yet to be well defined. It has been demonstrated that the oncogene *SALL4* upregulates Bmi1 through direct binding to its promoter in AML (Schuringa & Vellenga, 2010). Other genes which increase Bmi1 expression include sonic hedgehog (*Shh*) and microRNA 128 (*mir128*) (Schuringa & Vellenga, 2010). Within the sonic hedgehog pathway, sonic hedgehog binds to and inhibits Patched which releases inhibition on Smoothened allowing it to enter the cell. There, it stimulates the Gli1 transcription factor to enter the nucleus and increase transcription of Bmi1 leading to inhibition of the *INK4A/ARF* locus and increasing cell proliferation and inhibiting apoptosis (Bruggeman *et al*., 2007; Valk-Lingbeek *et al*., 2004). However, much work still remains to determine other Bmi1 regulatory mechanisms and pathways which may influence cancer progression.

The current study aims to investigate the effect of Bmi1 knockdown on glioblastoma stem-like cells. *In vitro* as well as *in vivo* analysis of Bmi1 knockdown will be performed in order to determine the effect of Bmi1 on self-renewal and proliferation. We hypothesize that the loss of Bmi1 will result in decreased self-renewal and proliferation *in vitro* and decreased glioblastoma brain tumour formation *in vivo*.

Chapter 2.

METHODS

All work with live cells, including animal work, was carried out in Class II Biological Safety hoods.

2.1 Tumour Dissociation, RBC Lysis, Cell Feeding

Primary brain tumour samples were obtained from consenting patients following Hamilton Health Sciences/McMaster Health Sciences Research Ethics Board guidelines. Samples were collected from both the Hamilton General Hospital and McMaster University Medical Centre. Primary brain tumour samples were dissociated in artificial cerebrospinal fluid with 200µL Liberase Blendzyme3 (0.2 Wünsch units/ml, Roche) and placed on an incubator shaker (VWR) at 37^{o}C for 15 minutes. The dissociated tissue was then filtered through a 70µm cell strainer (BD) and the resulting solution was centrifuged at 290 g for 5 minutes. Supernatant was removed and red blood cells were lysed using ammonium chloride solution (Stem Cell Technology) previously warmed to 37^{o}C. After 5 minutes of incubation at room temperature, the sample was centrifuged at 290 g for 5 minutes. Supernatant was removed, and cells were washed once with PBS (Hyclone). After PBS wash, the pelleted cells were resuspended and plated in an ultra-low attachment plate (Corning) in serum-free neural stem cell media (Tumour Sphere Medium). Complete neural stem cell media is composed of neural stem cell basal media (1% N2 supplement (Gibco), 0.2% 60µg/mL N-acetylcystine (Sigma), 2% neural survival factor-1 (Lonza), 1% HEPES (Wisent), and 6mg/mL glucose (Sigma) in 1:1 DMEM:F12 media (Gibco)), supplemented with human recombinant EGF (20ng/ml; Sigma), bFGF (20ng/ml; Invitrogen), LIF (10ng/ml; Chemicon), and antibiotic and antimycotic solution (Wisent). Cultures were incubated at 37^{o}C, 5% CO_2 and fed every other day.

2.2 Secondary Sphere Formation Assay

A single-cell suspension was prepared by dissociating tumour spheres with 5-10μL of Liberase Blendzyme3 (0.2 Wünsch units/ml, Roche) in 1mL PBS for 5-10 minutes at 37°C. Cells were counted using trypan blue exclusion dye (Invitrogen) with the Countess Automated Cell Counter (Invitrogen). A solution of 2000 live cells/mL of neural stem cell media was used to prepare dilutions ranging from 200 cells/100μL to 2 cells/100μL; for each dilution, four replicates of 100μL were plated in a 96-well ultra-low attachment plate (Corning). Cultures were left undisturbed at 37°C for one week, after which the number of spheres per well were counted. The secondary sphere formation rate was calculated from the number of spheres forming from 2000 dissociated cells to quantify stem cell frequency.

2.3 Sphere Size Assay

Sphere size from the secondary sphere formation assay was used as a measure of cellular proliferation within cells (Tropepe *et al*., 1999). Spheres from wells of the secondary sphere formation assay were imaged using an Olympus IX81 microscope at day 7 post-plating (Model: IX-1LL100LH) and sphere diameter was measured using the callipers tool on the Metamorph software. Five sphere diameter measurements were taken and average sphere size was determined.

2.4 Proliferation Assay

A single-cell suspension was prepared as described previously. Cells were counted as described previously and 500 live cells/well were plated under two distinct conditions: serum-free neural stem cell media (Tumour Sphere Medium) and basal neural stem cell media with 10% FBS (Hyclone) and antibiotics. Triplicates of each condition were plated in 5 plates (Day 0, Day 3, Day 5, Day 7, and Day 10). On each respective day, plates were centrifuged at 290 g for 5

minutes and media was removed from plates. The plates were then frozen at -80^{o}C for a minimum of 24 hours. Once all plates were frozen down, the cell proliferation assay was performed using the CyQuant Cell Proliferation Kit (Invitrogen) and 400-fold diluted CyQuant dye in 1x cell lysis buffer was added to each well and analysed using a FLUOstar Omega fluorescence Microplate reader (BMG LABTECH) at λ_{Ex}=485, λ_{Em}=525. The proliferation assay measures cell proliferation through the use of CyQuant dye which binds to nucleic acids and emits a fluorescent signal which can be detected to determine relative levels of nucleic acids.

2.5 Differentiation Assay and Cell Staining

For flow cytometric analyses of differentiation, cells from cultures were plated in a 6-well flat-bottom plate (Falcon) in basal neural stem cell media with 20% FBS (Hyclone) and antibiotics. After 7 days of differentiation, media was removed and wells were washed once with PBS. Trypsin (0.05% in 0.53mM EDTA; Invitrogen) was added to each well and incubated at 37^{o}C for 5 minutes. PBS was added and cells were collected. Cells were centrifuged at 290 g for 5 minutes and resuspended in fresh PBS. Cells were counted and aliquots of 100,000 cells/100µl were placed into the appropriate number of flow tubes (BD Falcon) and centrifuged at 290 g for 5 minutes. Cells were resuspended in 100µL of PBS with 2mM EDTA (Sigma). Conjugated antibodies for CD133 surface staining and isotype control were added in the appropriate dilutions (Supplementary Table 1). After a 35 minute incubation on ice, cells were washed with PBS and 200µL of fix-perm solution (BD) was added to each tube. After a 20 minute incubation on ice, cells were washed with 1mL cytoperm buffer (BD) and resuspended in 100µL of cytoperm buffer. Intracellular antibodies and the appropriate isotype controls for Bmi1, MAP2 (neuronal marker), and GFAP (glial cell marker) were then added to the cells in the correct

concentrations (Supplementary Table 1). Cells were left to incubate with conjugated antibodies for 45 minutes on ice. Cells were washed with 2mL of cytoperm buffer and resuspended in 250µL of PBS with 2mM EDTA. Stained cells were then analysed using the MoFlo XDP (Beckman Coulter).

For immunofluorescence staining of differentiated cells, cells from culture were suspended as single cells and plated on coverslips (Fisher Scientific) (25,000 live cells/coverslip), previously coated in a 1:10 dilution of Matrigel (BD Biosciences) in a 24-well flat-bottom plate (Falcon), in basal neural stem cell media with 20% FBS (Hyclone) and antibiotics. After 7 days of differentiation, a 4% solution of PFA (Falcon) was added to each well and incubated at room temperature for 10 minutes. The PFA solution was removed and the wells were washed gently with PBS. A 0.1% Triton X solution (Sigma) was then added to each well as a permeabilisation buffer for 15 minutes at room temperature. The permeabilisation buffer was removed and the wells were washed with PBS twice. A 1.5% goat serum solution in PBS (Santa Cruz) was added to each well as a blocking agent and left to incubate at room temperature for 1 hour. Antibodies targeting internal antigens MAP2 and GFAP were then added using the appropriate dilutions (Supplementary Table 1; conjugated MAP2, unconjugated primary GFAP). Plates were covered with foil and left at 4^{o}C overnight. The following morning, antibodies were removed and cells were washed using wash buffer (BD Biosciences). Washing was done three times for 5 minutes each time on an incubator shaker (VWR) which was gently rocking. Secondary antibodies were added and after 30-45 minutes of incubation in the dark, cells were washed three times for 5 minutes each time on an incubator shaker with wash buffer (BD Bioscience). A Hoechst solution (1:20,000) was added to each well and incubated in the dark for 10 minutes at room temperature followed by a PBS wash. Coverslips were removed using forceps, rinsed with water, and

mounted on slides using fluorescent mounting media (Dako). Slides were visualized using an Olympus IX81 fluorescent light microscope (Model: IX-1LL100LH).

2.6 Flow Cytometry and Cell Sorting

Flow cytometry allows us to analyse huge numbers of individual cells as well as recover specific populations of interest through sorting. The fluidics system of a cytometer is responsible for aligning the cells in single file. This is achieved through the interaction of sheath fluid moving through a flow cell at a faster velocity than an injected cellular suspension. This difference in velocity creates pressure on the cellular suspension and forces it into a stream of single cells. This process is termed hydrodynamic focusing (Rahman, 2009). After this focusing, the cells may pass through one or more lasers beams and the scattered laser light and/or fluorescence of each particle is collected by photomultiplier tube detectors. The laser light scattered in a forward direction, or Forward Scatter, provides a relative measurement of cell size while scattered light measured at a 90^{o} angle reveals information about the granular content (Rahman, 2009). These two parameters are frequently used together to visualise a sample's distribution and allows gating out of cellular debris and possible doublets. A series of optical filters separate the fluorescence light emitted. Fluorescence signals may have a wide distribution of intensity and are generally displayed on a log scale so that weak signals are expanded and strong signals are compressed allowing both to be plotted graphically (Rahman, 2009). Once the gates are set, cells can be analysed and displayed as single-parameter histograms of count versus fluorescence intensity or two-parameter dot plots, in which each dot represents a single "event" or cell's distribution for the staining parameters. For cell sorting, the sheath stream is vibrated so that droplets are formed. When the desired cell or particle reaches the position of the last attached

droplet the fluid stream is electrostatically charged and the charged droplet is directed either left or right by voltage plates into a collection tube (Rahman, 2009).

For flow cytometry, a single-cell suspension was prepared as described previously and single cells were suspended in PBS with 2mM EDTA (Sigma). Cells were then stained according to staining protocol described previously using conjugated antibodies (Supplementary Table 1). For cell sorting based on GFP expression, a single-cell suspension was prepared and cells were suspended in complete neural stem cell media for sorting. One hour after sorting, cells were centrifuged at 244 g for 3 minutes and plated in 24-well ultra-low attachment plate (Corning) in complete neural stem cell media.

2.7 Viral Knockdown

Lentiviral constructs CS-H1-Bmi1shRNA-EF-1 -EGFP expressing short hairpin RNA (shRNA) which target Bmi1 ***1*** (Target sequence: **5'-GAGAAGGAATGGTCCACTT-3'**) and CS-HI Luc shRNA-EF-1 –EGFP expressing the targeting sequence for Luciferase (as a negative control), were a kind gift to the Singh lab from Professor Atsushi Iwama (Chiba *et al*., 2008).

Knockdown validation was carried out with three lentiviral constructs expressing shRNA (Genecopoeia). Lentiviral constructs used included shBmi1 ***2*** (Target location: 1015, Target sequence: **5'-GACTGTGATGCACTTAAGA-3'**), shBmi1 ***3*** (Target location: 1091, Target sequence: **5'-GAGGAGGAACCTTTAAAGG-3'**), shBmi1 ***4*** (Target location: 507, Target sequence: **5'-TGCATCGAACAACGAGAAT-3'**), and a scrambled control. Bmi1 DNA targets can be found in Supplementary Figure 1.

2.7.1 Plasmid DNA Extraction

Plasmid DNA was received from Dr. Iwama (shBmi1 ***1***, shLuc) and from Genecopoeia (shBmi1 ***2***, shBmi1 ***3***, shBmi1 ***4***, shControl (scramble control)) on filter discs. For DNA extraction from

the filter discs, 20µL of TE (10:1 Tris:EDTA, pH 8.0; Promega, Sigma) buffer was added to the finely cut discs and incubated at room temperature for 20 to 30 minutes. The solution was then vortexed and centrifuged at 580 g for 3 minutes. Supernatant containing plasmid DNA was then removed and used for transformation. *E.coli* cells, DH5alpha, (Invitrogen SKU# 18265-017) were used for transformation. 50µL aliquots of DH5alpha cells were placed in an ice-cold eppendorf tubes (Fisher Scientific). For each sample, 5µL of extracted plasmid DNA was added to the DH5alpha cells and mixed gently by tapping the eppendorf tube. The pUC 19 plasmid was used as a positive control and water was used as a negative control. Cells were incubated on ice for 30 minutes followed by a heat shock in a 42^{o}C water bath for 20 seconds. Cells were then placed back on ice for 2 minutes. Next, 950µL of warm super optimal broth with catabolite repression (SOC) media was added to each eppendorf tube and incubated at 37^{o}C on an incubator shaker, set to 0.7 g, for one hour. Following incubation, 20-200µL of each transformed *E.coli* cells were plated on LB agar plates containing 100µg/mL of ampicillin. The LB agar plates were incubated at 37^{o}C in an inverted position overnight. The following day, isolated colonies were inoculated individually in 5 mL LB broth with ampicillin. After 8 hours of incubation, each culture was transferred to 100 mL LB broth with ampicillin for MaxiPrep of plasmid DNA. MaxiPrep was carried out using the Plasmid DNA MaxiPrep Kit (Norgen Biotek). Lysate was prepared by centrifuging 100 mL of the bacterial culture containing the plasmid DNA at 6000 g for 15 minutes. Supernatant was carefully removed and cells were resuspended in 6 mL of Resuspension Buffer containing RNAse. The cellular suspension was incubated for 15 minutes at room temperature. Following incubation, 6 mL of lysis solution was added to the suspension and gently mixed in by inverting the tube repeatedly until the solution turned clear indicating that the cells had lysed. 6 mL of Neutralization Solution was immediately mixed in.

The solution was centrifuged at 14,000 g for 10 minutes to pellet out the insoluble particles and clarify the lysate. The supernatant containing the lysate was transferred to a filter column assembly and centrifuged in a swinging bucket rotor centrifuge at 3000 g for 5 minutes to remove any remaining particles. To the clarified lysate, 2 mL of Binding Solution was added and mixed well. 200µL of Endotoxin Removal Solution was mixed in well and left to incubate at room temperature for 5 minutes. Then, 2 mL of Isopropanol was added to the solution and mixed in by vortexing. The lysate was then applied to the reservoir of the spin column assembly and centrifuged in a swinging bucket rotor centrifuge at 3000 g for 5 minutes. The flowthrough was discarded and the spin column was reassembled with the collection tube. To the column assembly, 15 mL of Wash Solution was added and the assembly was centrifuged at 3000 g for 10 minutes. Then, 0.5 mL of Elution Buffer was added to the column and the unit was centrifuged at 3000 g for 5 minutes. The collection tube was discarded and a small amount of the Elution Buffer was passed through the column. A fresh 50 mL Elution Tube was attached to the column containing the resin bound DNA and 2 mL of Elution Buffer was added to the centre of the resin bed. The column was centrifuged at 3000 g for 5 minutes. The DNA was quantified using Nanodrop spectrophotometer and 260/280 ratio was noted for purity of the sample. Agarose gel electrophoresis was performed to verify the DNA.

2.7.2 Production of Virus

Lentiviral constructs were generated using the HEK (Human Embryonic Kidney) 293 FT cell line. HEK 293 FT cells were plated on seven 100mm tissue culture plates (BD Falcon) and grown in DMEM high glucose media supplemented with Na pyruvate, NEAA, L-glutamate, 10% FBS, and 1µL/mL Geneticin antibiotic (500µg/ml, Invitrogen). Cells were passaged twice before beginning transfection. The DNA concentration (shBmi1 ***1***-***4***, shLuc or scramble control) used

for the constructs for each plate was 3µg. As well, each plate received 9µL of Virapower Packaging Mix (Invitrogen) containing pLP1, pLP2, and pLP/VSVG packaging plasmids at 1µg/µl in TE buffer and 36µL of Lipofectamine 2000 (Invitrogen) suspended in 3mL of optiMEM media (Invitrogen). One plate was used as a control plate and no DNA was added. Plates were then topped up with 7mL of optiMEM media and placed in the BSL2+ lentivirus incubator (37^{o}C, 5% CO_2). Cells were left with constructs overnight (24h) and the media was removed and replaced with 10ml HEK media without antibiotics. 48-72 hours post-transfection, the control plate was observed under fluorescence microscope to confirm no GFP present and discarded. Supernatants were centrifuged at 1811 g for 15 minutes at 4^{o}C to pellet out debris. Supernatants were then transferred to new Falcon tubes and filtered through a Millex-HV 0.45um PVDF filter. The viral suspension was then centrifuged at 115,993 g and 4^{o}C for 2 hours. The supernatant was discarded and each pellet was resuspended in 1mL PBS. Each virus type was then aliquoted into 10 cryovials (100µL/cryovial) and frozen at -80^{o}C in a locked freezer.

2.7.3 Titration of Virus

Transduction of Daoy medulloblastoma cell line was performed in order to determine the multiplicity of infection (MOI) for each virus. Daoy cells were plated in a regular 6-well tissue culture plate such that there were 40 000 cells/well in ATCC MEM media. On day 2, the media was changed on all wells and 10^{-2} dilutions (10µL) as well as 10^{-3} dilutions (1µL) of each virus were used to determine the respective MOIs. Media was changed 24 hours later. On day 4, GFP expression was analysed by flow cytometry on the MoFlo XDP (Beckman Coulter).

The MOI was calculated based on the 10^{-3} dilution as follows:

Lentiviral titer (# of Transduction Units/mL) = cell number (on day of transduction) x fraction of transduced cells x dilution factor

2.7.4 Transduction of Cells

Knockdown of cells was carried out using calculated titer for both shLuc and shBmi1.

Common MOI from literature is 1-10 TU/cell (Multiplicity of Infection) – An MOI of 5 was used for knockdowns using shBmi1 ***1*** and shLuc and an MOI of 2 was used for knockdowns using shBmi1 ***2-4*** and shControl.

Virus required for knockdown= (MOI x number of cells) ÷ lentiviral titer

Tumour spheres were dissociated with 10µL of Liberase Blendzyme3 (0.2 Wünsch units/ml, Roche) in 1mL PBS for 10 minutes at 37°C, then plated in single cell suspension on ultra-low attachment plate (Corning) in serum-free neural stem cell media (Tumour Sphere Medium). Virus was added drop wise to the cells in the amount calculated using the MOI and the viral titer. Cells were left to incubate overnight at 37^{o}C, 5% CO_2. The following day, the media was changed and the cells were left for another 24 hours before being analysed for GFP expression on the MoFlo XDP (Beckman Coulter). If GFP expression was greater than 80% in cells, the population of cells was considered enriched for transduction and cells were used unsorted. If GFP expression was less than 80%, cells were sorted for GFP positive cells in order to select for an enriched population.

2.8 Real-Time Polymerase Chain Reaction

Real-Time Polymerase Chain Reaction was performed by Dr. Chitra Venugopal of the Singh lab. Briefly, total RNA from samples was isolated using the Qiagen RNeasy Micro kit (Qiagen) and reverse transcribed using Superscript III First Strand Synthesis kit (Invitrogen). Quantitative PCR was performed using the Chroma4 (Bio-Rad) with iQSYBR Green qPCR kit (Quanta). Data are presented as the ratio of the gene of interest to GAPDH (glyceraldehyde-3-phosphate dehydrogenase) as control.

2.9 Western Blot

Western blots were performed by Dr. Chitra Venugopal of the Singh lab. Briefly, denatured total protein (20 mg) was separated using 10% sodium dodecyl sulphate-polyacrylamide gel electrophoresis and transferred to polyvinylidene fluoride membrane. Western blots were probed with monoclonal mouse-anti-human Bmi1antibody (Upstate) and anti-GAPDH antibody (Abcam). The secondary antibody was horseradish peroxidase-conjugated goat anti-mouse IgG (HþL) (Bio-Rad) in a dilution of 1:15 000. Bands were visualized using an Immobilon Western kit (Millipore).

2.10 Intracranial Injection

A single-cell suspension was prepared by dissociating tumour spheres with 5-10µL of Liberase Blendzyme3 (0.2 Wünsch units/ml, Roche) in 1mL PBS for 5-10mins at 37°C. Cells were counted using trypan blue exclusion dye (Invitrogen) with the Countess Automated Cell Counter (Invitrogen). The desired cell number was then aliquoted into eppendorf tubes (Fisher Scientific) and centrifuged at 10,621 g for 3 minutes. The supernatant was removed and cells were resuspended in 10µl PBS. Cells were put on ice and brought to the McMaster Stem Cell Unit (SCU) for intracranial injection.

NOD/SCID gamma (NSG) immunocompromised mice (NOD.Cg-*Prkdc*^{scid} *Il2rg*^{tm1Wjl}/SzJ) aged 4-8 weeks were weighed and either anaesthetized with the appropriate dosage of tribromoethanol (Avertin: 0.018ml/g; Sigma) via intraperitoneal injection or anaesthetized using gas anaesthesia (Isoflurane: 2.5%; Pharmaceutical Partners of Canada). Once unresponsive, mice were positioned in stereotaxic frame (Stoelting) and the top of the head was swabbed with iodine. A 1.5 cm vertical midline incision was made using a 15-blade knife down to the periosteum. The knife blade was then used to clear the periosteum. Using a drill held perpendicular to the skull, a

small burr hole was created at the point of injection (2-3 mm anterior to coronal suture, 3 mm lateral to midline). A Hamilton syringe was used to inject 10µl of cell suspension into the frontal lobe. The syringe was inserted through the burr hole at a 30 degree angle to a 5 mm depth. Once cells were injected, the injection site was cleared using a gauze square and gentle pressure was applied to prevent bleeding. The incision was closed using 5.0 dexon (Ethicon) interrupted stitches and sutures were sealed with Vetbond tissue adhesive (3M). Mice were then injected subcutaneously with 0.5 mL temgesic (Buprenorphine: 0.3 mg/mL; Schering-Plough) and 1 mL saline. Mice were identified using ear notches and placed in recovery cages in front of heat lamps until awake. The following morning, mice were given 0.5 mL temgesic (Buprenorphine: 0.3 mg/mL; Schering-Plough) subcutaneously. Mice were monitored weekly for signs of illness.

2.11 Animal Collection, Sectioning and Staining

Mice were monitored for signs of illness (weight loss, lethargy, ruffled appearance, gray skin tone, withdrawal from cage mates, etc) and when endpoint appeared imminent, mice were euthanized and brains were collected via perfusion. The mouse was anaesthetized with the appropriate dosage of tribromoethanol (Avertin: 0.020ml/g; Sigma) via intraperitoneal injection. Once unresponsive, the mouse was taped down on an absorbent pad with the thorax and abdomen exposed. The torso was sprayed with ethanol and the fur was cut away. The abdomen and thorax were then opened by holding the skin upwards and away from the organs while cutting. The diaphragm was very carefully cut, exposing the heart. An 18-gauge needle attached to a gravity feedbag of saline was inserted through the apex of the heart and into the left ventricle. The tubing valve was opened to allow saline to flow into the heart. The posterior vena cava was immediately cut to allow blood to escape. The saline was flushed through the system until the exit fluid was clear, approximately 8 minutes. The saline valve was closed and the

needle was switched over to a 30 mL syringe containing 10% formalin. The 10% formalin solution was slowly injected into the heart and circulated throughout the body. Once perfused, the head was cut from the body and the brain was carefully removed. First, all skin was cut away and the skull was carefully peeled away using tissue forceps (Magna). The isolated brain was then suspended in 10% Formalin for a minimum of 48 hours before sectioning.

After 48 hours, brains were placed in the sectioning frame and the first blade was inserted into the first slit at the posterior end of the brain. A second blade was then placed in the third slit and the first blade was removed. The first section of tissue was disposed of and the blade was then placed in the fifth slit, the blade from the third slit was then removed and the section of tissue was placed in a tissue cassette. Sectioning continued in this manner, with sections being cut every 2 slits until the brain was completely sectioned and the 6 sections were in the tissue cassette. The cassette was then placed in 70% ethanol and sent to histology for paraffin wax embedding and H&E staining.

2.12 Statistical Analysis

Unless otherwise stated, all comparisons were performed using unpaired, two-tailed student t-tests or ANOVA tests with Bonferroni Post-Hoc tests. Statistical significance was set at 0.05.

2.13 Sample numbers

Sample numbers (n) represent technical or experimental replicates unless otherwise stated.

Chapter 3.

RESULTS

3.1 BT 241 Characterization

Brain tumour sample number 241 (BT 241) was received on April 26, 2010 from a female patient aged 68. Final pathology indicated that the tumour sample was a Glioblastoma which was post therapy and had radiation effects and atypia (recurrent/residual). Immunohistochemistry performed by the pathologist showed areas of GFAP positivity, high Ki-67 proliferation (40-50%) and strong diffuse nuclear positivity of p53. In culture, BT 241 was highly proliferative and as a result developed into a spontaneous "cell line" which has remained stable after multiple passages and has been frozen down and revived successfully (Figure 1). BT 241 was the primary sample used for all *in vitro* and *in vivo* work. Stem cell assays were performed on BT 241 in order to characterize the "cell line" for our use.

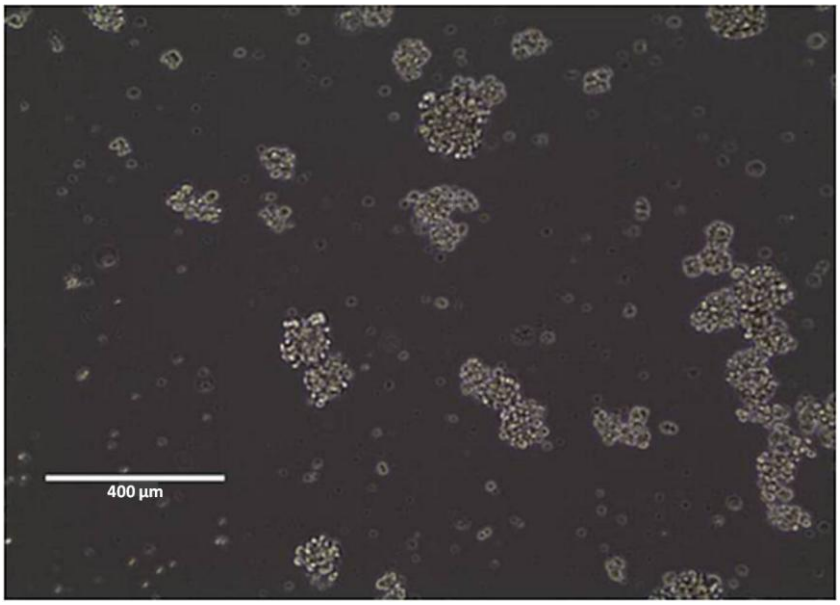

Figure 1. BT 241 culture

3.1.1 Flow Analysis and Differentiation

Flow cytometry analysis was conducted on BT 241 (n=3) to analyse levels of Bmi1, neural stem cell marker CD133 (Singh *et al*., 2003; Singh *et al*.,2004a; Tabatabai & Weller, 2011; Uchida *et al*., 2000), neuronal marker MAP2, and astrocyte marker GFAP under both neural stem cell culture conditions as well as differentiation culture conditions. Representative flow plots can be found in Supplementary Figure 2.

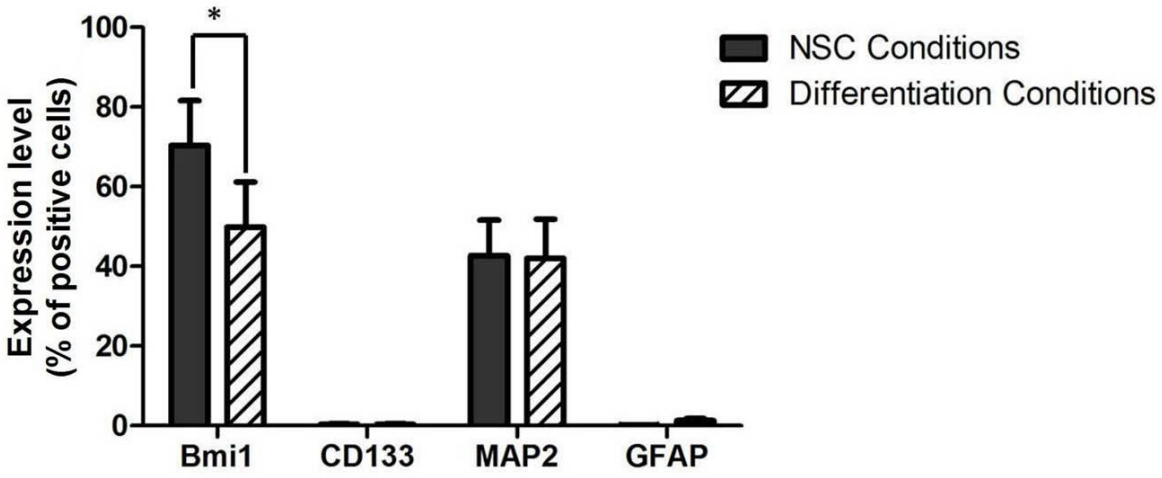

Figure 2. Expression levels (measured as percentage of positive cells) of Bmi1, CD133, MAP2, and GFAP for BT 241 under neural stem cell culture conditions and differentiation conditions. Under differentiation conditions, BT 241 showed significantly less Bmi1 expression than neural stem cell conditions. No differences were seen for CD133, MAP2, or GFAP levels. Data represented as mean ± SD (n=3).

The results indicated that under differentiation conditions, Bmi1 levels were significantly less than levels seen under neural stem cell culture conditions ($p<0.05$, Figure 2). No significant

differences were found for CD133, MAP2, or GFAP expression levels under either condition (Figure 2). MAP2, a marker of mature neurons, expression was 42.72% and 42.07% for NSC and differentiation conditions, respectively. GFAP, a marker of mature astrocytes, expression was 0.12% 1.33% for NSC and differentiation conditions, respectively. MAP2 expression was much greater than GFAP expression under both conditions indicating that BT 241 is more neuronal in phenotype (Figure 2).

3.1.2 Secondary Sphere Formation

Secondary sphere formation was analysed and sphere formation per 2000 cells was plotted for BT 241 (n=3) and three other primary GBM tumour samples (n=1)

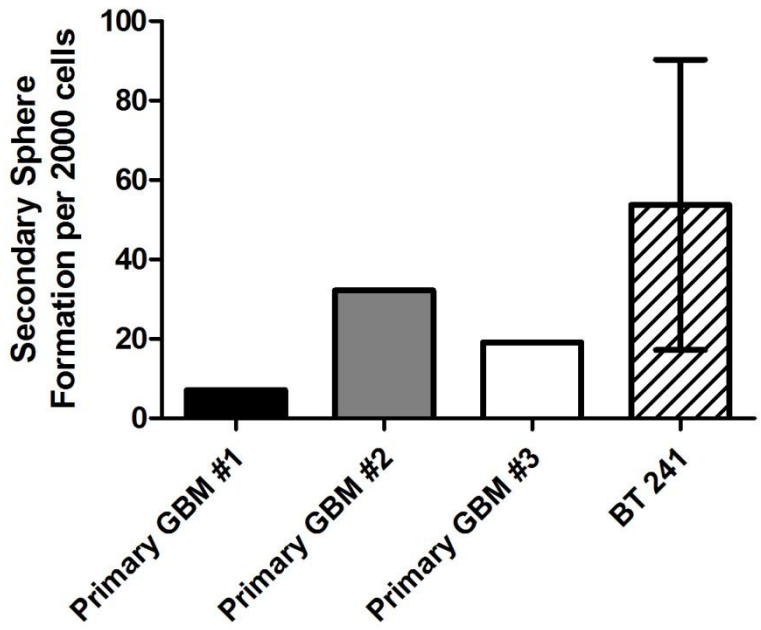

Figure 3. Secondary sphere formation of BT 241 appears similar to 3 primary GBMs. BT 241 secondary sphere formation was greater (53.75 ± 21.12) than three primary GBMs (7.15 – 32.24). Data represented as mean ± SD (1^{o} GBM n=1, BT 241 n=3).

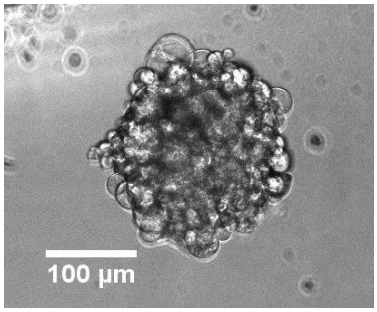

Figure 4. BT 241 sphere. Average sphere size was 119.67 µm.

BT 241 sphere formation was 53.75 ± 21.12 (n=3) while the sphere formation for three other primary GBMs ranged from 7.15 to 32.24 (n=1). BT 241 spheres were measured as a representation of proliferation. The average sphere size for BT 241 was 119.67 µm in diameter (Figure 4).

3.1.3 Proliferation

BT 241 cells (500 cells/well) were plated for proliferation assays (n=3). Proliferation of cells was analysed at days 0, 3, 5, 7, and 10. Proliferation was assessed under neural stem cell conditions, in complete neural stem cell media and under serum conditions, in basal media with 10% FBS (Figure 5).

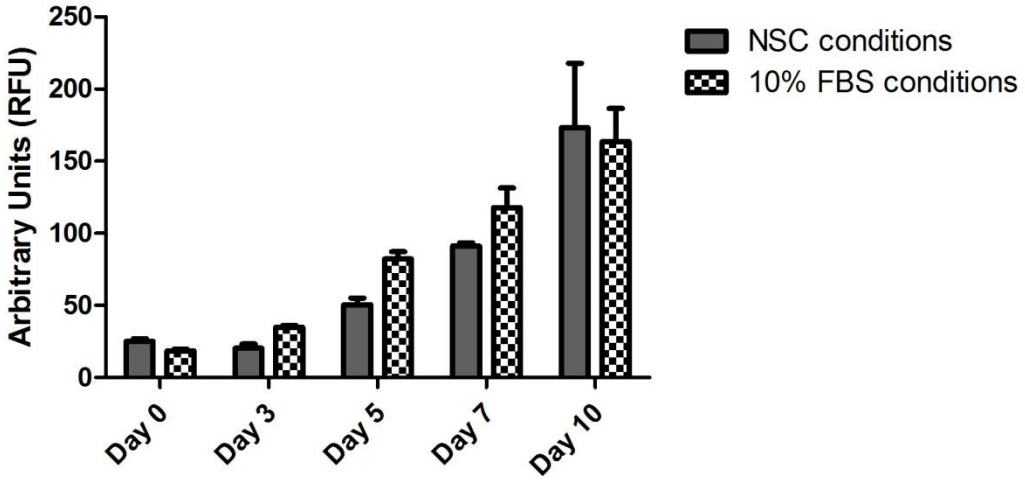

Figure 5. Proliferation of BT 241 cells (500 cells/well). BT 241 cells plates for proliferation analysis showed increased proliferation from Day 0 to Day 10. No difference was found between neural stem cell conditions and 10% FBS conditions. Data represented as mean ± SD (n=3).

The proliferation assay measures cell proliferation through the use of CyQuant dye which binds to nucleic acids and emits a fluorescent signal which can be detected to determine relative levels of nucleic acids. Proliferation of BT 241 cells appeared to increase over time in both NSC and serum conditions (Figure 5). Proliferation did not differ significantly between culture conditions ($p>0.05$, Figure 5).

3.2 BT 241 Knockdown with shLuc and shBmi1 *1*

BT 241 tumour spheres were transduced with shLuc and shBmi1 ***1*** lentiviral vectors. Following the validation of transduction using flow cytometric analysis of GFP expression (Figure 6), *in*

vitro experiments were performed on unsorted, enriched cells to maintain high cell number and viability.

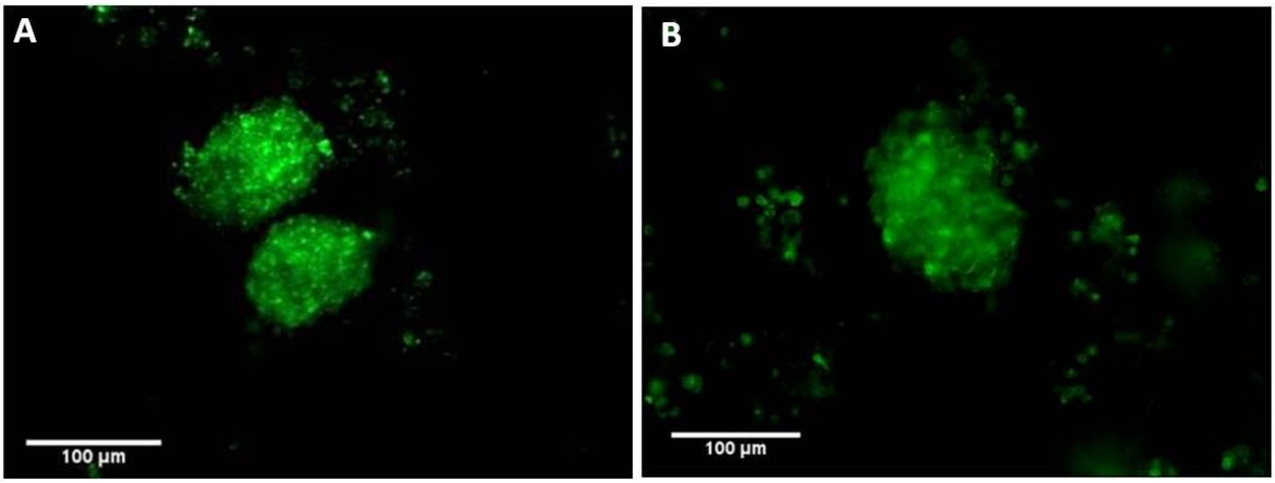

Figure 6. GFP expression of A: BT 241 shLuc cells, B: BT 241 shBmi1 cells

3.2.1 Knockdown Validation

Lentiviral constructs shLuc and shBmi1 ***1*** were previously validated by the Singh lab in various cell lines such as U2OS (Human Osteosarcoma) and Daoy (Human Medulloblastoma). Bmi1 knockdown in BT 241 was confirmed through RT-PCR which demonstrated significant reductions in Bmi1 mRNA in transduced cells (Figure 7). Western blot analysis of BT 241 shLuc and shBmi1 ***1*** cells further confirmed significant Bmi1 knockdown at the protein level (Figure 8). U20S lysate was used as a positive control.

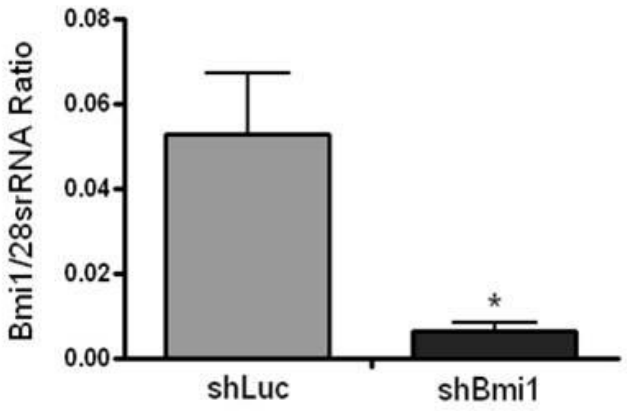

Figure 7. Bmi1 mRNA levels were significantly decreased in cells transduced with shBmi1 *1* as compared to cells transduced with shLuc. Data represented as mean ± SD (n=3).

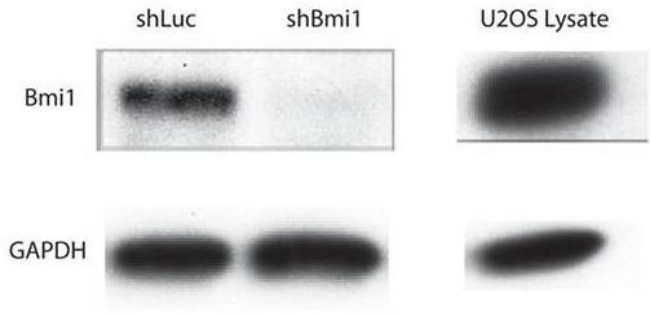

Figure 8. Bmi1 protein levels were decreased in cells transduction with shBmi1 *1* as compared to cells transduced with shLuc.

3.2.2 Flow Analysis

Flow cytometric analysis of BT 241 knockdown using shLuc (n=1) and shBmi1 ***1*** (n=1) was conducted to evaluate the expression levels of Bmi1 and neural stem cell markers CD133 and CD15. Representative flow plots can be found in Supplementary Figure 3.

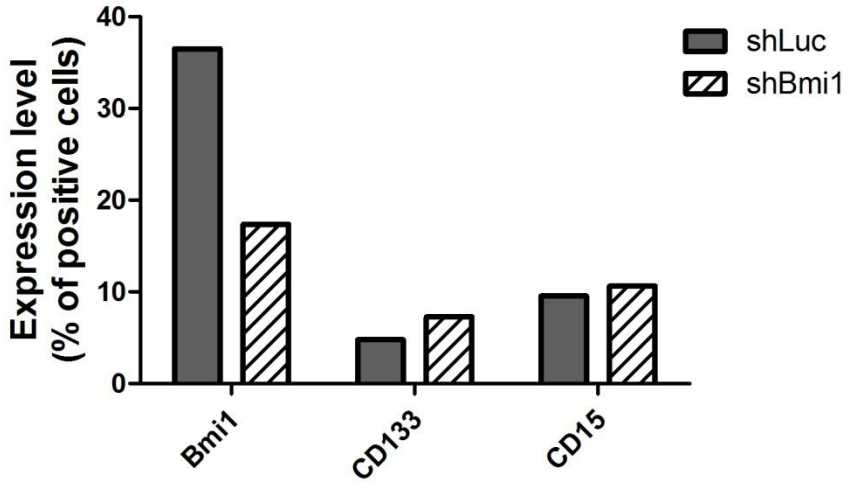

Figure 9. Expression levels (measured as percentage of positive cells) of Bmi1, CD133, and CD15 for BT 241 shLuc and shBmi1 *1*. BT 241 shBmi1 cells showed less Bmi1 expression than shLuc cells. CD133 levels appeared decreased in shLuc cells as compared to shBmi1 cells. CD15 levels appeared similar in both groups. Data represented as mean (n=1).

The flow analysis of BT 241 knockdown cells indicated a decrease in Bmi1 in shBmi1 ***1*** cells as compared to shLuc cells (Figure 9). An increase in CD133 population within shBmi1 ***1*** cells was also observed while the CD15 populations in both shLuc and shBmi1 ***1*** appeared very similar

(Figure 9). These observed differences were not statistically analysed as this experiment was only performed once.

3.2.3 Secondary Sphere Formation

Secondary sphere formation of BT 241 cells transduced with shLuc and shBmi1 ***1*** was analysed (n=3) and sphere formation per 2000 cells was plotted (Figure 10). Average sphere size was also determined from day 7 spheres and analysed as a measure of proliferation (Figure 11).

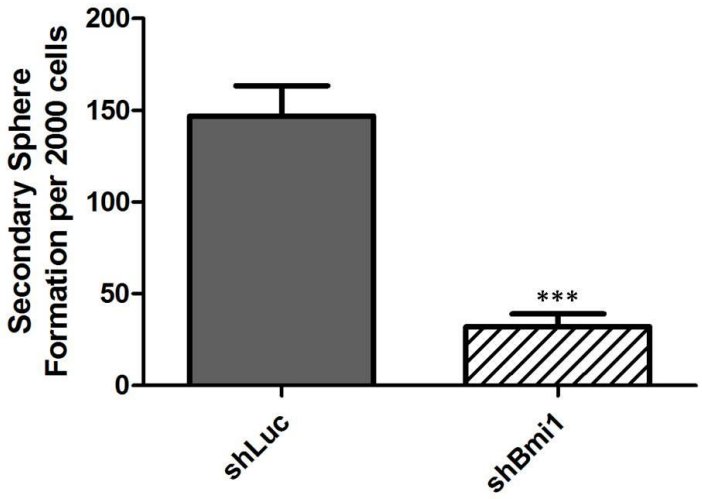

Figure 10. BT 241 shBmi1 *1* cells exhibited decreased self-renewal compared to shLuc cells. BT 241 shBmi1 cells showed decreased sphere formation per 2000 cells (32 ± 7.051) than shLuc cells (146.9 ± 16.53). Data represented as mean ± SD (n=3).

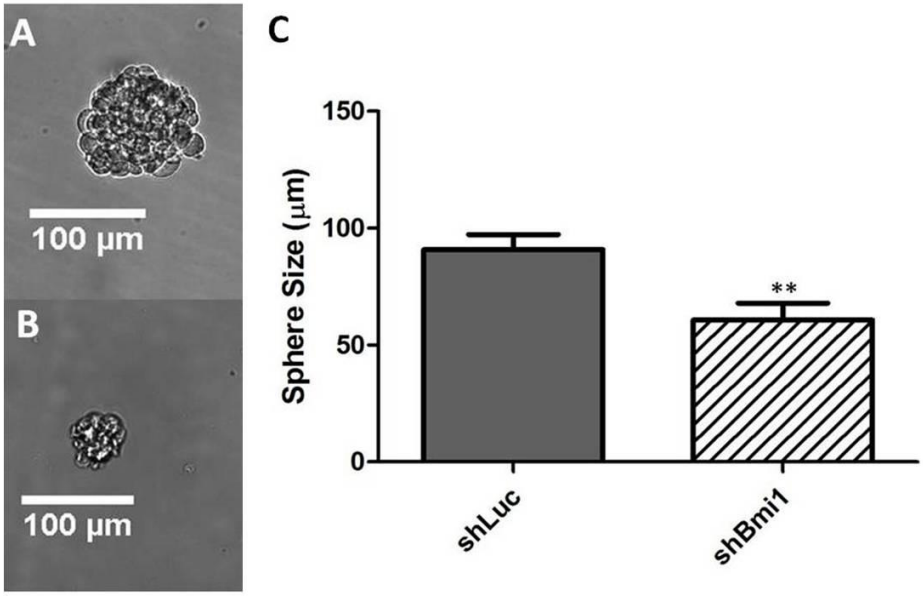

Figure 11. Sphere size (µm) was decreased in BT 241 shBmi1 *1* spheres compared to shLuc spheres. (A) BT 241 shLuc spheres were larger (90.84 µm) than (B) shBmi1 spheres (60.68 µm) and this difference was statistically significant (C). Data represented as mean ± SD (n=3).

Secondary sphere formation analysis revealed that Bmi1 knockdown significantly decreased self-renewal capacity of BT 241 cells (p=0.0004; Figure 10). The shBmi1 ***1*** spheres were smaller (60.68µm) than shLuc spheres (90.84µm) throughout the secondary sphere formation assays and this difference was found to be statistically significant (p=0.0058; Figure 11).

3.2.4 Proliferation

BT 241 shLuc and shBmi1 ***1*** cells (500 cells/well) were plated for proliferation assay (n=3). Proliferation of cells was analysed at days 0, 3, 5, 7 and 10. Proliferation was assessed under serum conditions, in basal media with 10% FBS (Figure 12).

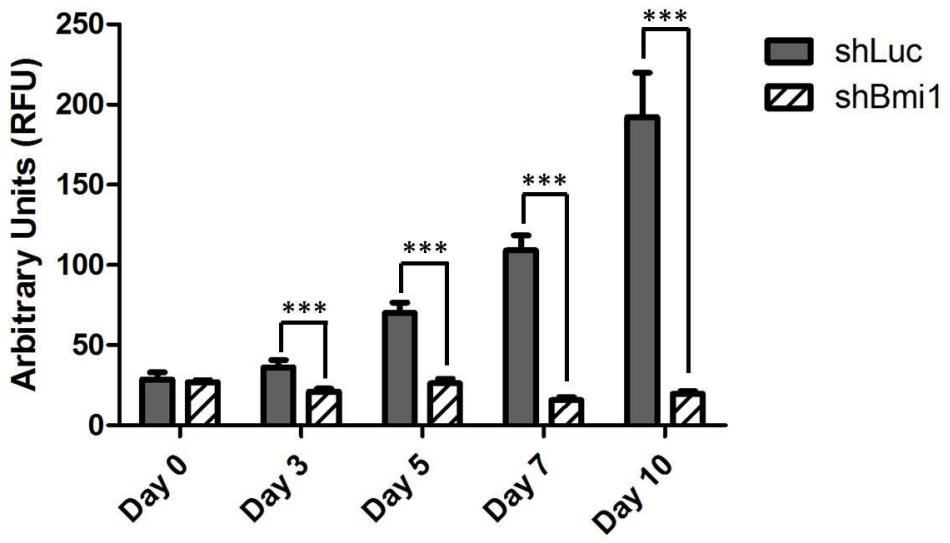

Figure 12. BT 241 shBmi1 *1* cells exhibited decreased proliferation under serum conditions compared to shLuc cells (500 cells/well). BT 241 shLuc cells plated for proliferation analysis showed increased proliferation from Day 0 to Day 10. No increase in proliferation was seen in shBmi1 ***1*** cells from Day 0 to Day 10. Data represented as mean ± SD (n=3).

Proliferation of Bmi1 knockdown cells was significantly decreased as compared to control cells at Day 3, Day 5, Day 7, and Day 10 ($p<0.001$, Figure 12). While proliferation of shLuc cells increased over time, proliferation of Bmi1 knockdown cells appeared relatively equal at all time points (Figure 12).

3.2.5 Differentiation

BT 241 shLuc and shBmi1 ***1*** cells were plated in single cell suspension in basal neural stem cell media with 20% FBS and antibiotics for differentiation (n=1). After 7 days of differentiation,

cells were analysed qualitatively by immunofluorescence staining using the conjugated antibody for MAP2 and the unconjugated antibody for GFAP and quantitatively by flow cytometry using the conjugated antibody for MAP2 and the conjugated antibody for GFAP (Supplementary Table 1).

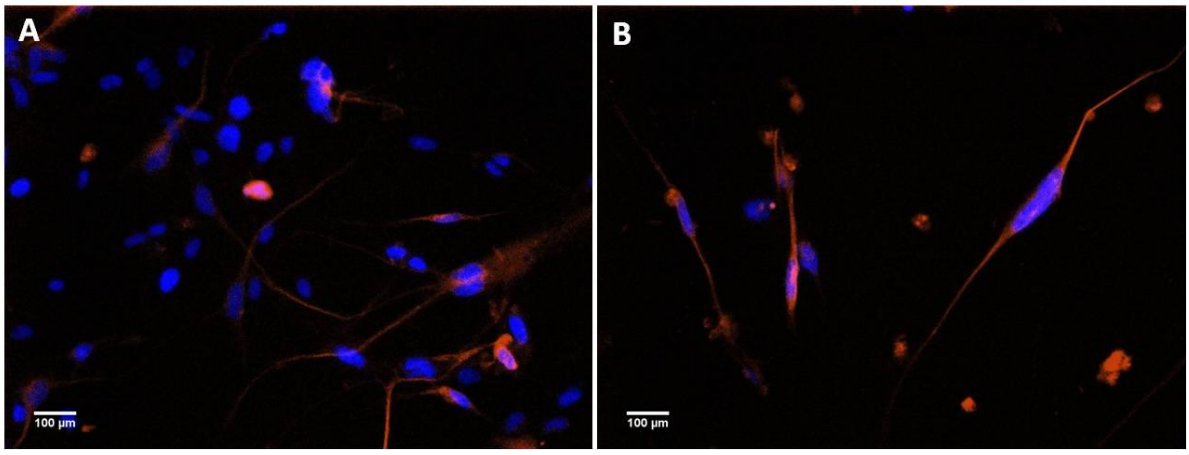

Figure 13. Neuronal differentiation of A: BT 241 shLuc cells and B: BT 241 shBmi1 *1* cells stained with anti-MAP2

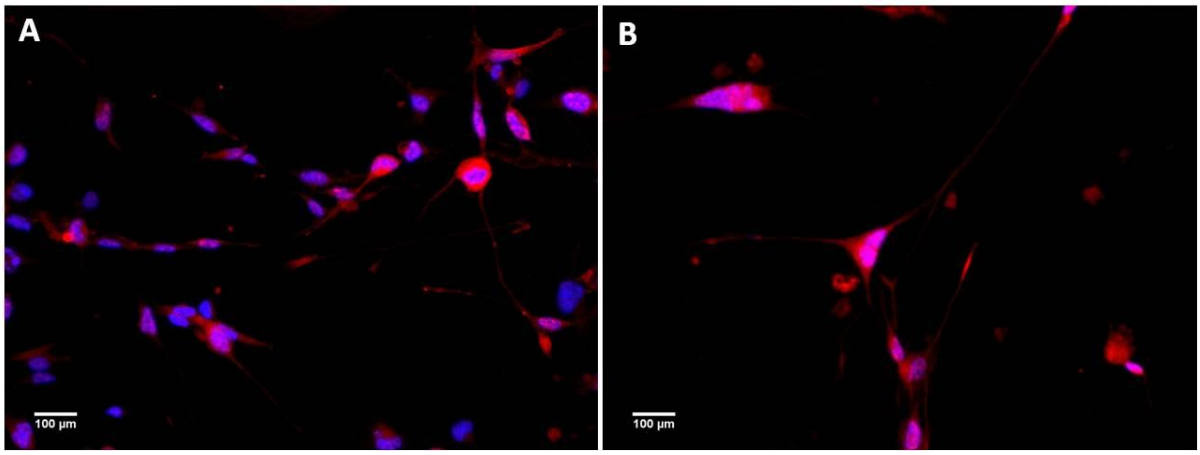

Figure 14. Glial differentiation of A: BT 241 shLuc cells and B: BT 241 shBmi1 *1* cells stained with anti-GFAP

Immunofluorescence staining of BT 241 shLuc and shBmi1 ***1*** cells was inconclusive as GFAP staining appeared to mark all cells, even cells which had a bipolar neuronal morphology (Figure 14). As a result, immunofluorescence staining was not used as a quantitative measure of differentiation and cells were analysed by flow cytometry for differentiation markers (Figure 15) using antibodies validated for flow cytometric analysis (Supplementary Table 1).

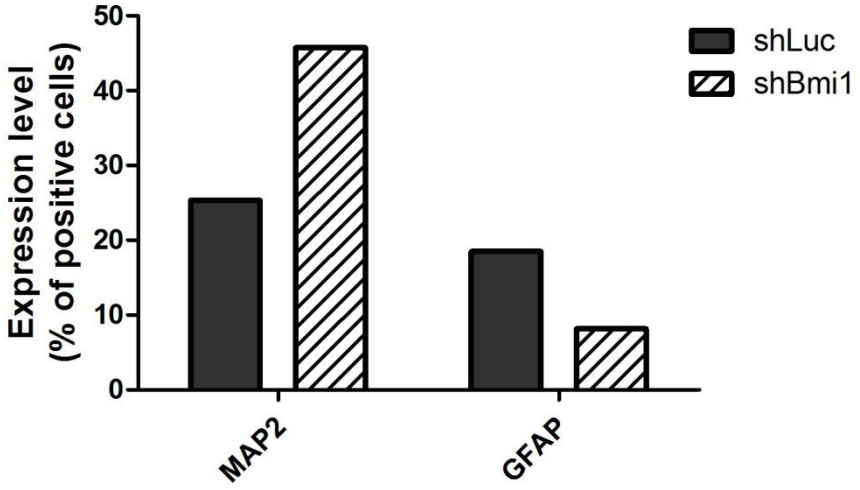

Figure 15. Differentiation marker expression levels (measured as percentage of positive cells) for BT 241 shLuc cells and shBmi1 *1* cells. BT 241 shBmi1 cells showed increased neuronal differentiation and decreased glial differentiation compared to shLuc cells. Data represented as mean ± SD (n=1).

Flow analysis of differentiated BT 241 shLuc cells and shBmi1 ***1*** cells (n=1) indicated greater neuronal differentiation, marked by MAP2 staining, than glial differentiation, marked by GFAP staining (Figure 15). Neuronal differentiation appeared greater in shBmi1 ***1*** cells than shLuc cells while glial differentiation appeared greater in shLuc cells than shBmi1 ***1*** cells (Figure 15). These

observed differences were not statistically analysed as this experiment was only performed once. Representative flow plots can be found in Supplementary Figure 4.

3.3 U-118 MG Knockdown with shLuc and shBmi1 *1*

The commercial GBM cell line U-118 MG (ATCC, cat. # HTB-15) was used to assess Bmi1 knockdown using shLuc and shBmi1 ***1*** lentiviral vectors. Following the validation of Bmi1 knockdown and validation of an enriched population of GFP positive cells, *in vitro* experiments were performed on unsorted cells to maintain high cell number and viability.

3.3.1 Knockdown Validation

Lentiviral constructs shLuc and shBmi1 ***1*** were validated by the Singh lab and Bmi1 knockdown was confirmed through RT-PCR which demonstrated significant reductions in Bmi1 mRNA in transduced cells (Figure 16). Untransduced U-118 MG cell mRNA was analysed to confirm that the shLuc control was a proper control (Figure 16).

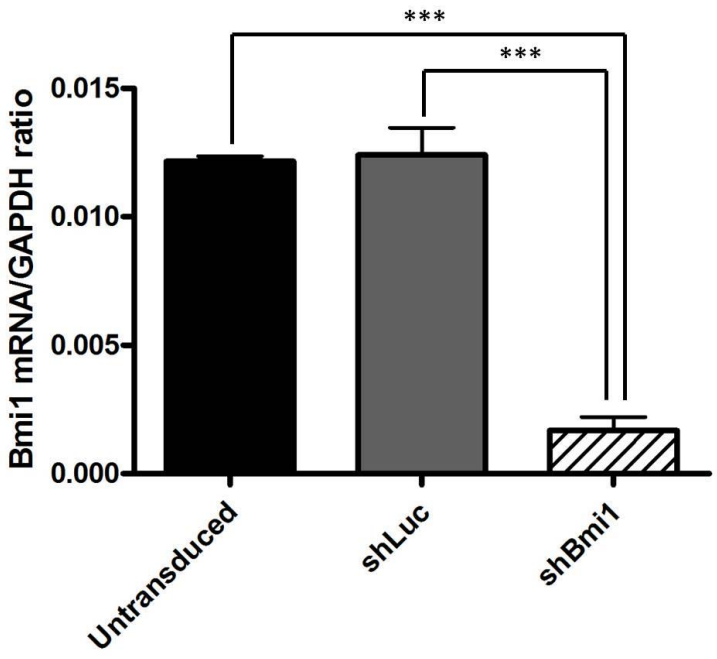

Figure 16. Bmi1 mRNA levels were significantly decreased in U-118 MG shBmi1 *1* cells compared to untransduced and shLuc cells. Data represented as mean ± SD (n=4).

3.3.2 Secondary Sphere Formation

Secondary sphere formation of U-118 MG transduced with shLuc and shBmi1 ***1*** was analysed (n=3) and sphere formation per 2000 cells was plotted (Figure 17). Average sphere size was also determined from day 7 spheres and analysed as a measure of proliferation (Figure 18).

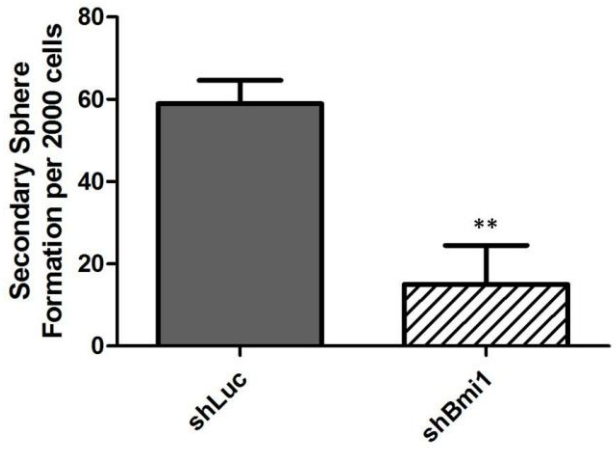

Figure 17. U-118 MG shBmi1 *1* cells exhibited decreased self-renewal compared to shLuc cells. U-118 MG shBmi1 cells showed decreased sphere formation per 2000 cells (15.05 ± 9.422) than shLuc cells (58.99 ± 5.625). Data represented as mean ± SD (n=3).

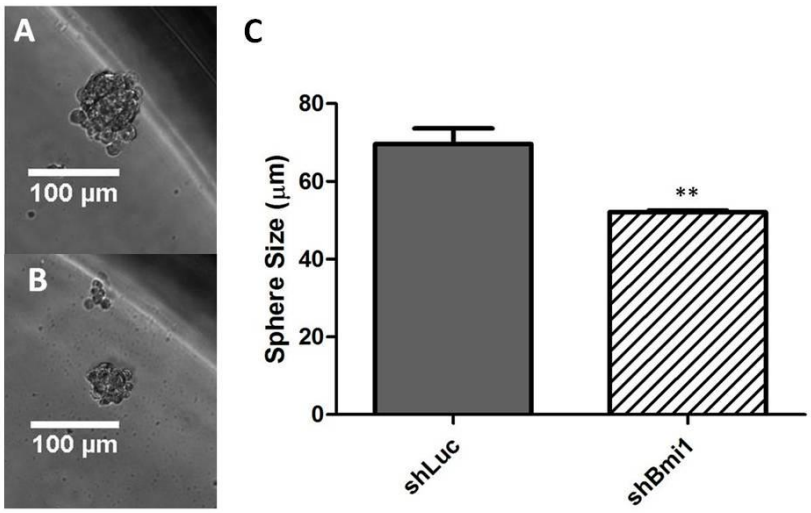

Figure 18. Sphere size (µm) was decreased in U-118 MG shBmi1 *1* spheres compared to shLuc spheres. (A) U-118 MG shLuc spheres were larger (69.65 µm) than (B) shBmi1 spheres (52.13 µm) and this difference was statistically significant (C). Data represented as mean ± SD (n=3).

Secondary sphere formation analysis revealed that Bmi1 knockdown significantly decreased self-renewal capacity of U-118 MG cells (p=0.0023; Figure 17). The shBmi1 ***1*** spheres were smaller (52.13µm) than shLuc spheres (69.65µm) throughout the secondary sphere formation assays and this difference was found to be statistically significant (p=0.0016; Figure 18).

3.3.3 Proliferation

U-118 MG shLuc and shBmi1 ***1*** cells (500 cells/well) were plated for proliferation assay (n=3). Proliferation of cells was analysed at days 0, 3, 5, 7 and 10. Proliferation was assessed under serum conditions, in basal media with 10% FBS (Figure 19).

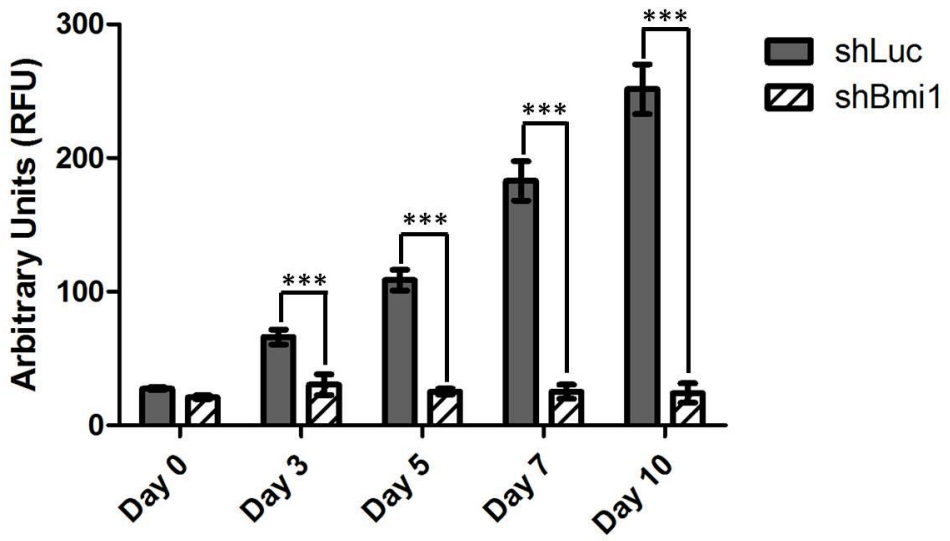

Figure 19. U-118 MG shBmi1 *1* cells exhibited decreased proliferation under serum conditions compared to shLuc cells (500 cells/well). U-118 MG shLuc cells plated for proliferation analysis showed increased proliferation from Day 0 to Day 10. No increase in proliferation was seen in shBmi1 ***1*** cells from Day 0 to Day 10. Data represented as mean ± SD (n=3).

Proliferation of Bmi1 knockdown cells was significantly decreased as compared to control cells at days 3, 5, 7, and 10 ($p<0.001$, Figure 19). While proliferation of shLuc cells increased over time, proliferation of Bmi1 knockdown cells appeared to remain similar at all time points (Figure 19).

3.3.4 Differentiation

U-118 MG shLuc and shBmi1 ***1*** cells were plated in single cell suspension in basal neural stem cell media with 20% FBS and antibiotics for differentiation (n=1). After 7 days of differentiation, cells were analysed qualitatively by immunofluorescence staining using the conjugated antibody for MAP2 and the unconjugated antibody for GFAP and quantitatively by flow cytometry using the conjugated antibody for MAP2 and the conjugated antibody for GFAP (Supplementary Table 1).

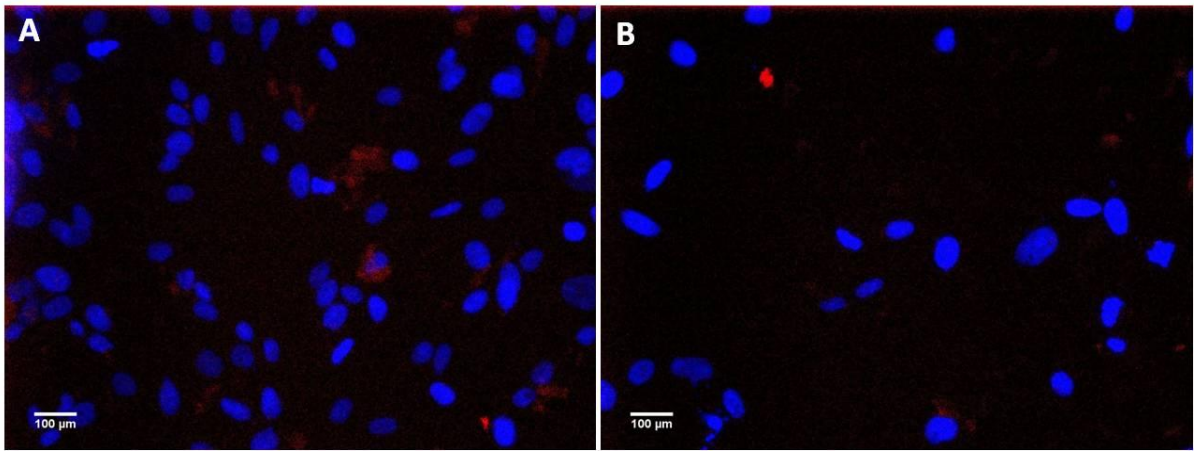

Figure 20. Neuronal differentiation of A: U-118 MG shLuc cells and B: U-118 MG shBmi1 *1* cells stained with anti-MAP2

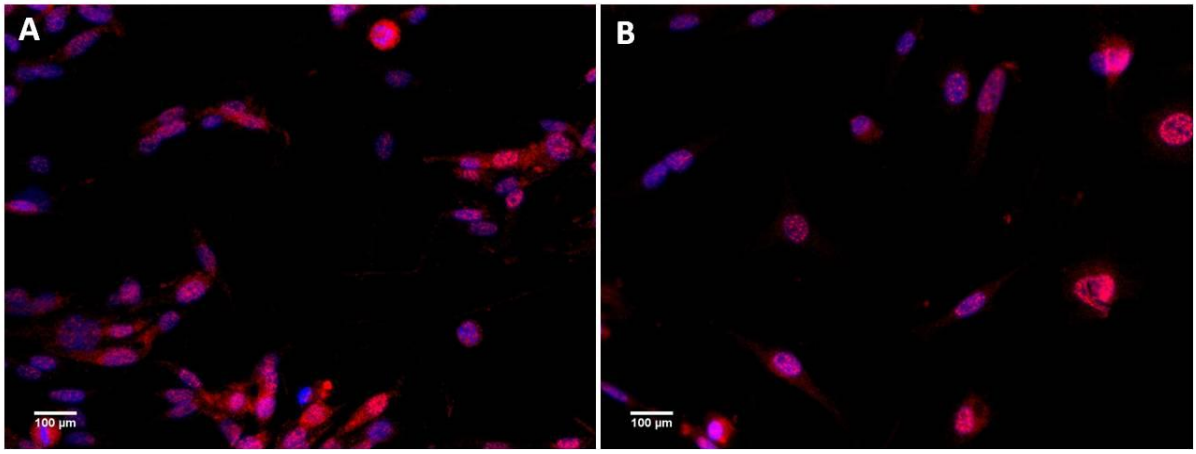

Figure 21. Glial differentiation of A: U-118 MG shLuc cells and B: U-118 MG shBmi1 *1* cells stained with anti-GFAP

Immunofluorescence staining of U-118 MG shLuc and shBmi1 ***1*** cells was inconclusive as MAP2 staining did not integrate into cells and GFAP staining appeared to mark all cells, even cells which had a bipolar, neuronal morphology (Figure 20 & 21).This may have been a result of unhealthy cells which appeared to be without normal cellular processes (Figure 20 & 21). As a result, immunofluorescence staining was not used as a quantitative measure of differentiation and cells were analysed by flow cytometry for differentiation markers (Figure 22) using antibodies validated for flow cytometric analysis (Supplementary Table 1).

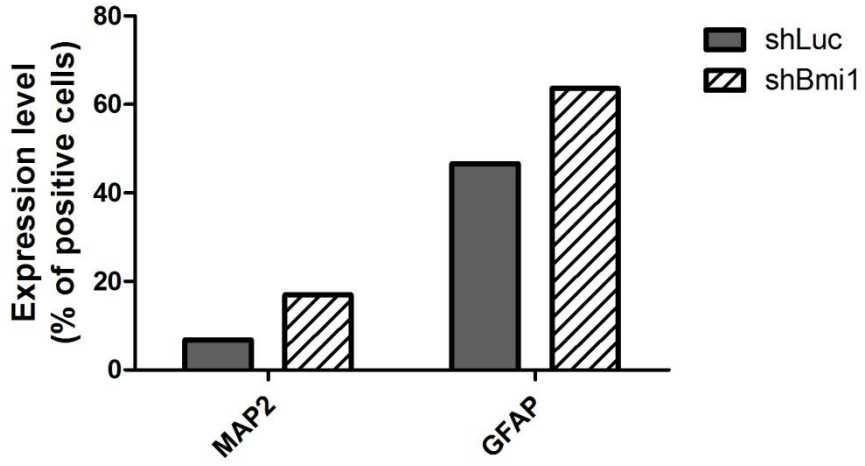

Figure 22. Differentiation marker expression levels (measured as percentage of positive cells) for U-118 MG shLuc cells and shBmi1 *1* cells. U-118 MG shBmi1 cells showed increased neuronal and glial differentiation compared to shLuc cells. Data represented as mean ± SD (n=1).

Flow analysis of differentiated U-118 MG shLuc cells and shBmi1 ***1*** cells (n=1) indicated greater glial differentiation marked by GFAP staining than neuronal differentiation marked by MAP2 staining (Figure 22). Both neuronal and glial differentiation appeared greater in shBmi1 ***1*** cells than shLuc cells (Figure 22). These observed differences were not statistically analysed as this experiment was only performed once. Representative flow plots can be found in Supplementary Figure 5.

3.4 BT 241 Knockdown with shControl, shBmi1 *2*, shBmi1 *3*, and shBmi1 *4*

To validate Bmi1 knockdown using short-hairpin RNA, three lentiviral constructs expressing shRNA against Bmi1 (Genecopoeia) were used on BT 241. *In vitro* experiments using lentiviruses shBmi1 ***2-4*** and a scrambled control (shControl) were conducted using unsorted BT 241 transduced cells to maintain high cell number and viability. GFP expression for each construct was analysed by flow cytometry and each population showed greater than 80% GFP positivity indicating enrichment for Bmi1 knockdown or scrambled control (Supplementary Figure 6).

3.4.1 Knockdown Validation

Knockdown was validated using the U-118 MG GBM cell line (ATCC, cat. # HTB-15). Bmi1 knockdown was not found to be efficient using any shBmi1 constructs in comparison to the scrambled control (Figure 23 & 24). To confirm the use of the scrambled control, we compared mRNA levels against our previously validated shLuc control mRNA (Figure 23). Protein levels were compared to untransduced U-118 MG cells (Figures 24). Against our validated shLuc control and untransduced cells, all shBmi1 constructs as well as the scrambled control (shControl) showed significantly decreased Bmi1 levels ($p<0.001$, Figure 23; no statistical analysis, Figure 24). From these observations, we doubted the validity of the scrambled control. Out of interest, all subsequent results were compared to previously acquired BT 241 shLuc data.

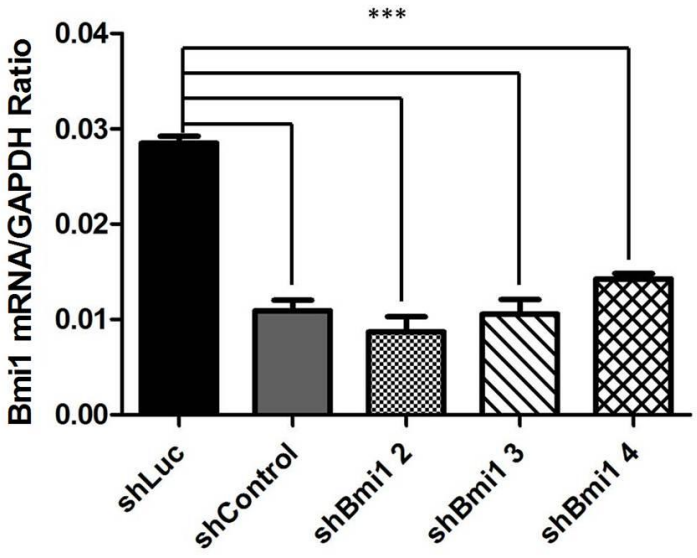

Figure 23. Bmi1 mRNA levels were significantly decreased in shControl, shBmi1 *2*, shBmi1 *3*, and shBmi1 *4* compared to shLuc cells. Data represented as mean ± SD (n=2).

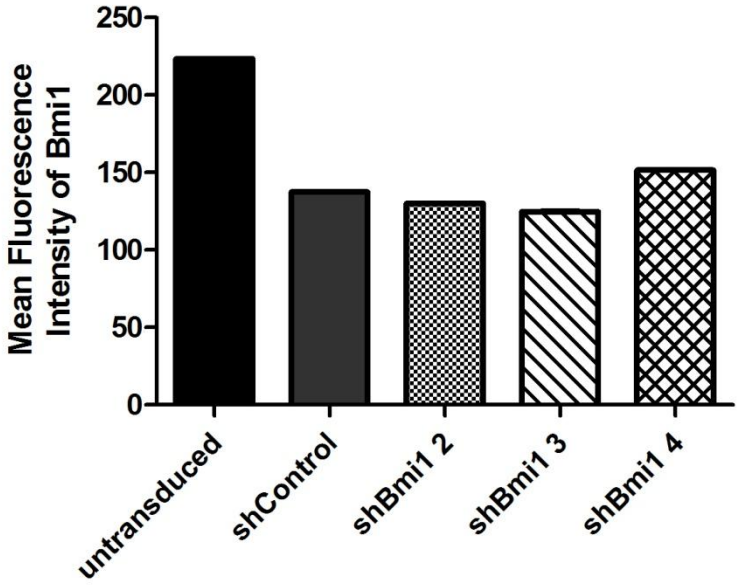

Figure 24. Bmi1 protein levels appeared decreased in shControl, shBmi1 *2*, shBmi1 *3*, and shBmi1 *4* compared to untransduced cells. Data represented as mean ± SD (n=1).

3.4.2 Secondary Sphere Formation

Secondary sphere formation assays were performed on BT 241 transduced with shControl, shBmi1 ***2***, shBmi1 ***3***, and shBmi1 ***4*** (n=3) and compared to previously acquired BT 241 shLuc secondary sphere formation data (n=2). Spheres were measured at day 7 for each population of cells (shControl, shBmi1 ***2***, shBmi1 ***3***, shBmi1 ***4***) (n=3) and the average sphere size was determined for each population.

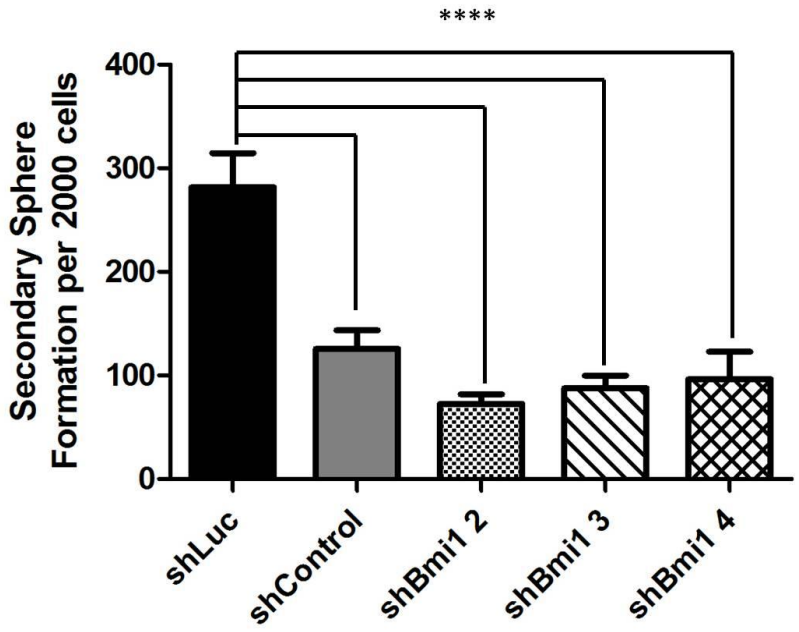

Figure 25. BT 241 shControl, shBmi1 *2*, shBmi1 *3*, shBmi1 *4* cells exhibited decreased self-renewal compared to shLuc cells. BT 241 shControl, shBmi1 ***2***, shBmi1 ***3***, and shBmi1 ***4*** cells showed decreased sphere formation per 2000 cells (72.49 – 125.5) than shLuc cells (281.3). Data represented as mean ± SD (shLuc n=2; shControl, shBmi1 *2-4* n=3).

Secondary sphere formation assays indicated an extremely significant effect of Bmi1 knockdown on secondary sphere formation for lentiviral constructs ***2***, ***3*** and ***4*** ($p<0.0001$, Figure 25) when compared to shLuc.

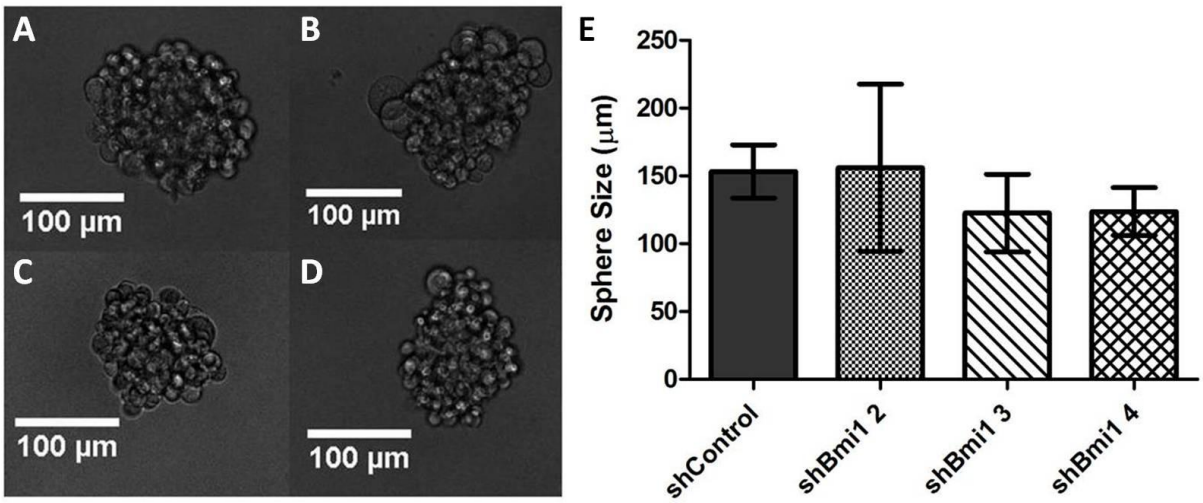

Figure 26. No differences in sphere size were seen between shControl and shBmi1 cells A: BT 241 shControl sphere, B: BT 241 shBmi1 *2* sphere, C: BT 241 shBmi1 *3* sphere, D: BT 241 shBmi1 *4* sphere, E: Average Sphere Size for BT 241 shControl and shBmi1 *2*, shBmi1 *3*, shBmi1 *4*. Data represented as mean ± SD (n=3).

Sphere size between each population was not found to be significantly different between shControl and any of the Bmi1 knockdown groups ($p>0.05$, Figure 26) with all spheres ranging from 122 µm to 153 µm (Figure 26).

3.4.3 Proliferation

BT 241 cells transduced with shControl, shBmi1 ***2***, shBmi1 ***3***, and shBmi1 ***4*** were plated for proliferation assays (n=3). Proliferation of cells was analysed at days 0, 3, 5, 7, and 10. Proliferation was assessed under neural stem cell conditions, in complete neural stem cell media (Figure 27), and under serum conditions, in basal media with 10% FBS (Figure 28).

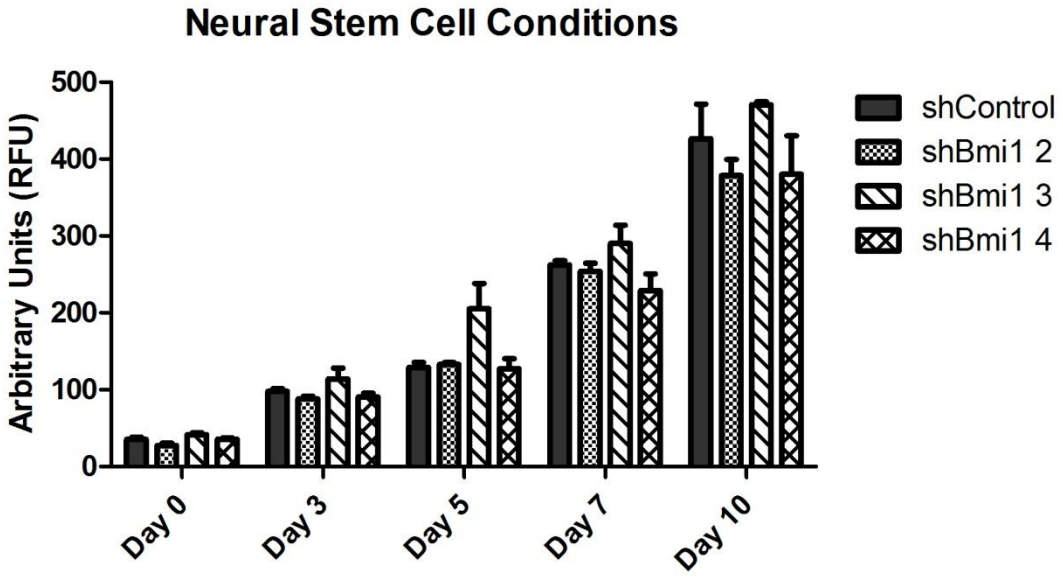

Figure 27. Proliferation of BT 241 shControl, shBmi1 *2*, shBmi1 *3*, and shBmi1 *4* under neural stem cell conditions. BT 241 shControl and shBmi1 cells plated for proliferation analysis showed increased proliferation from Day 0 to Day 10. No significant change was found between shControl cells and shBmi1 cells. Data represented as mean ± SD (n=3).

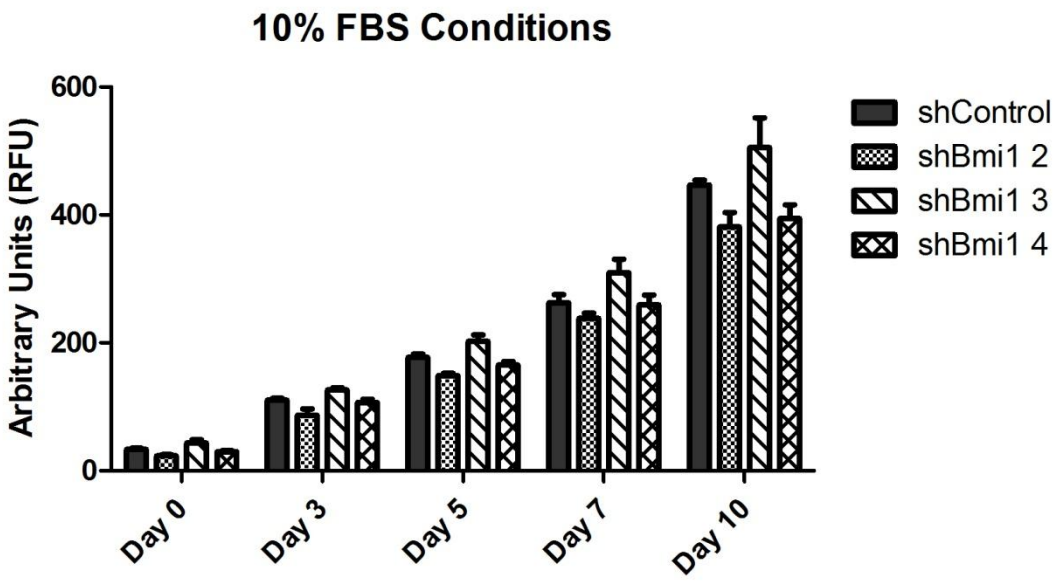

Figure 28. Proliferation of BT 241 shControl, shBmi1 *2*, shBmi1 *3*, and shBmi1 *4* under serum conditions. BT 241 shControl and shBmi1 cells plated for proliferation analysis showed increased proliferation from Day 0 to Day 10. No significant change was found between shControl cells and shBmi1 cells. Data represented as mean ± SD (n=3).

Proliferation of cells increased from Day 0 to Day 10 for both neural stem cell conditions and serum conditions. Both conditions showed similar proliferation profiles with no significant differences found (Figures 27 & 28).

3.4.4 Differentiation

BT 241 shBmi1 ***2-4*** and shControl cells (n=1) were placed under differentiation conditions for 10 days (Figure 29) and evaluated by flow cytometry. Expression levels of differentiation markers obtained were compared to previously acquired BT 241 shLuc differentiation data (Figure 30). Representative flow plots can be found in Supplementary Figures 4 & 7.

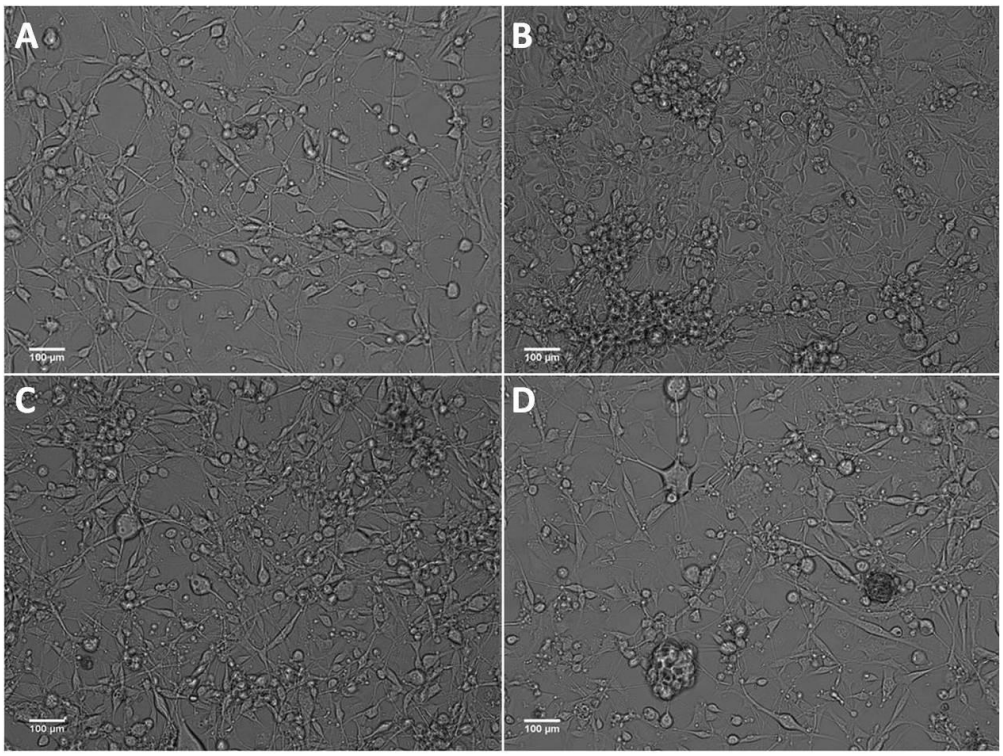

Figure 29. Differentiation of BT 241 cells transduced with A: shControl, B: shBmi1 *2*, C: shBmi1 *3*, D: shBmi1 *4*

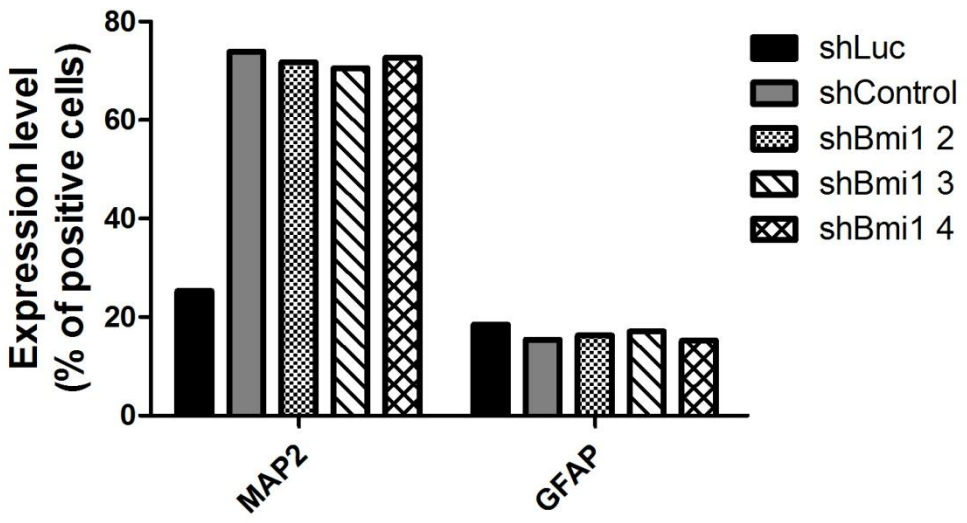

Figure 30. Differentiation marker expression levels (measured as percentage of positive cells) for BT 241 cells transduced with shLuc, shControl, shBmi1 *2*, shBmi1 *3*, and shBmi1 *4*. Neuronal (MAP2) differentiation appeared decreased in shLuc cells compared to shControl, shBmi1 ***2-4*** cells. Glial (GFAP) differentiation appeared similar in all groups. Data represented as mean ± SD (n=1).

When analysed by flow cytometry, levels of the neuronal marker MAP2 were extremely high (70.59%-73.88%) for cells transduced with shControl and shBmi1 ***2-4*** while levels of astrocyte marker GFAP were fairly low in all transduced cells (15.21%-18.5%) indicating a tendency towards the neuronal lineage (Figure 30). Interestingly, BT 241 shLuc cells expressed decreased MAP2 expression (25.33%) indicating less neuronal differentiation (Figure 30).

3.5 *In vivo* injection of BT 241 shLuc and shBmi1 *1* cells

BT 241 was transduced with GFP expressing shLuc or shBmi1 *1* lentiviral vectors as described in the Methods section. The enriched transduced cells or GFP positive cells which were sorted using the MoFlo XDP (Beckman Coulter) were used for *in vivo* injections in NSG mice as shown in Table 1. Once animals reached endpoint, they were collected and brains were sent to Dr. Kwiecien of McMaster University for pathological analysis. Table 1 describes all *in vivo* injections performed and the resulting pathology results.

Table 1. Intracranial injections of BT 241 cells transduced with shLuc and shBmi1 *1*

Number of Cells Injected	Number of Mice Injected for each Treatment	Number of shLuc Tumours	Number of shBmi1 Tumours
100	2	0	0
1000	2	1	0
5000	1	1	0
10,000	2	2	1
50,000	1	1	1
100 *sorted cells*	1	1	0
23,000 *sorted cells*	1	0	1

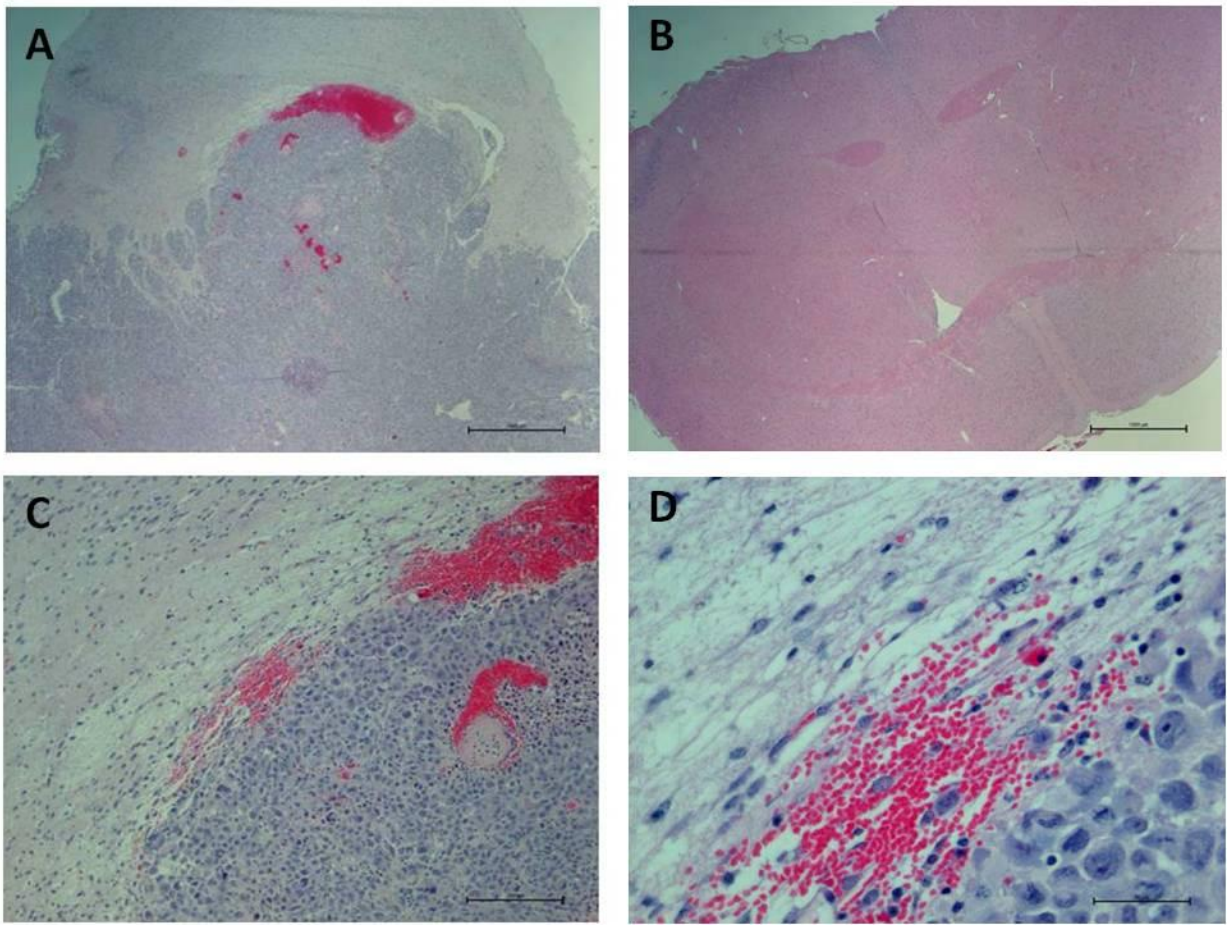

Figure 31. Tumour formation is absent in NSG mice injected with 100 sorted BT 241 shBmi1 *1* cells as compared to control cells. A: shLuc cells formed large, infiltrating masses (H&E stain), as seen in the prefrontal cortex (2X), B: shBmi1 cells formed no apparent tumours, C: shLuc tumours seen in the prefrontal cortex (10X) were accompanied by edema and haemorrhages, D: shLuc tumour showing haemorrhagic tissue (40X).

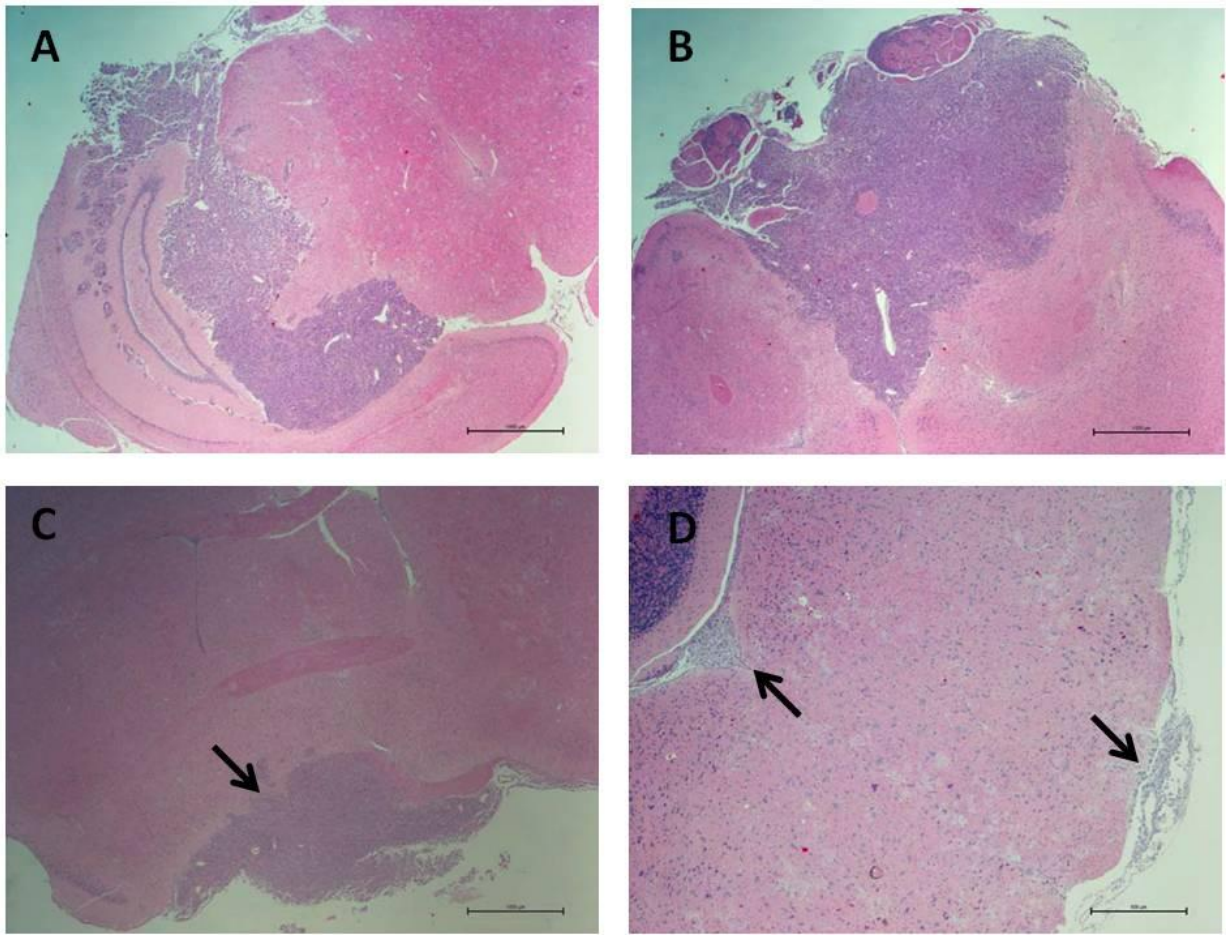

Figure 32. Tumour size appears decreased in NSG mice injected with BT 241 shBmi1 *1* cells compared to control cells. A: 10,000 BT 241 shLuc cells formed large, infiltrating masses, as seen in the midbrain (2X), B: 10,000 BT 241 shBmi1 ***1*** cells formed smaller, but still substantial, masses with moderate infiltration, as seen in the prefrontal cortex (2X), C: 50,000 BT 241 shLuc cells formed large, infiltrating masses as seen in striatum (2X), D: 50,000 BT 241 shBmi1 ***1*** cells formed smaller masses with mild to moderate infiltration, as seen in the fourth ventricle and medulla (4X).

Table 2. Relative tumour size of BT 241 cells transduced with shLuc and shBmi1 *1*

Number of Cells Injected	shLuc tumour size (mm^2)	shBmi1 *1* tumour size (mm^2)
10,000	18.03 (n=2)	5.3325 (n=2)
50,000	5.621 (n=1)	0.2679 (n=1)

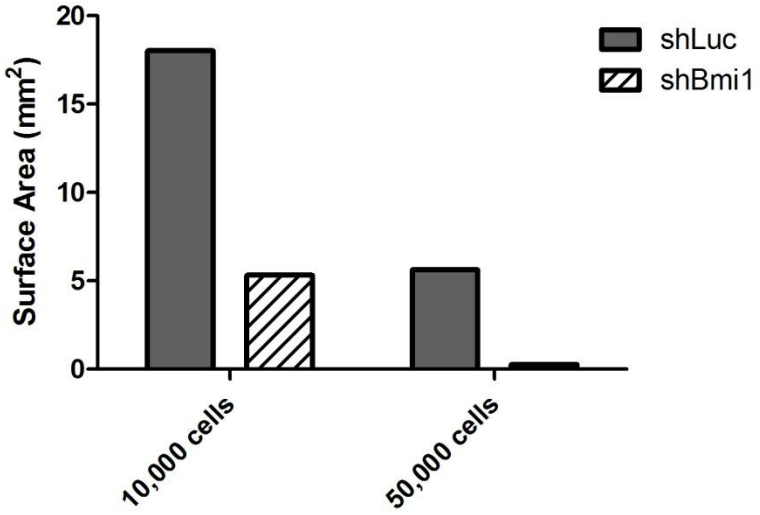

Figure 33. Tumour size (measured as surface area in mm^2) appeared smaller in BT 241 shBmi1 *1* cells compared to control cells. At both 10,000 and 50,000 cells, tumours formed from shBmi1 ***1*** cells had smaller surface areas than tumours formed from shLuc cells. Data represented as mean ± SD (10,000 cells n=2; 50,000 cells n=1).

Tumour formation was found in one NSG mouse injected with as low as 100 sorted BT 241 shLuc cells while no tumour formation was found in the corresponding NSG mouse injected with 100 sorted BT 241 shBmi1 cells (Figure 31). The appearance of tumours increased as cell number increased (Table 1). Although tumours were found in some mice injected with 10,000 and 50,000 BT 241 shBmi1 ***1*** cells, it was observed that tumours formed from shBmi1 ***1***

transduced cells showed moderate to mild infiltration by pleomorphic cells while shLuc transduced cells showed large tumour masses and increased infiltration (Figure 32). To determine whether tumour size was affected by Bmi1 knockdown, a relative surface area for tumours was measured for both shLuc and shBmi1 ***1*** tumours at 10,000 and 50,000 cells. Tumour size appeared decreased in shBmi1 ***1*** tumours at both cell numbers with tumour size ranging from 0.2679 mm^2 to 5.3325 mm^2 as compared to control tumours which ranged from 5.621 mm^2 to 18.03 mm^2 (Table 2). The decrease in shBmi1 ***1*** tumours compared to control tumours at 10,000 cells was not found to be statistically significant (Figure 33). The decrease in shBmi1***1*** tumour size as compared to shLuc tumours at 50,000 cells was not statistically analysed as there were not sufficient replicates (Figure 33).

Pathologically, all tumours were described as highly pleomorphic, with vascular endothelial hypertrophy, high mitotic index and of epithelial origin, consistent with the primary patient glioblastoma tumour.

Chapter 4.

DISCUSSION

Primary brain tumour sample 241, a glioblastoma tumour, was used for experimental conditions as it showed increased proliferation in culture and allowed for multiple experimental uses without overall depletion of cell number. Also, this sample did not undergo growth arrest in culture like most primary brain tumour samples. Flow analysis of BT 241 under neural stem cell conditions as well as differentiation conditions revealed a significant decrease in Bmi1 levels under differentiation conditions as compared to neural stem cell conditions (Figure 2). This result was expected as Bmi1 is a known developmental gene involved in stemness and vital for self-renewal and proliferation of stem cells (Abdouh *et al*., 2009; Ailles & Weissman, 2007; Bracken *et al*., 2006; Bruggeman *et al*., 2007; Chen *et al*., 2010; Fasano *et al*., 2007; Gil *et al*., 2005; Lessard & Sauvageau, 2003; Park *et al*., 2004). Thus it would be expected that as self-renewal decreases as a result of induced differentiation, levels of Bmi1 would decrease. It has been shown that during differentiation, PcG binding and H3K27me3 marks decrease as repression of gene transcription is released, allowing differentiation to occur (Bracken *et al*., 2006). Interestingly, when markers of differentiation, MAP2 and GFAP, were analysed under both neural stem cell conditions and differentiation conditions, no significant difference was found between either culture condition (Figure 2). This result was surprising as these differentiation markers were not expected under stem cell conditions. This may be an effect of long term culture of BT 241. Long term culture and spontaneous immortalization of cells may lead to differentiation block and presents a limitation of using cell lines. Furthermore, under both culture conditions, MAP2 expression was significantly higher than GFAP expression indicating differentiation was driven towards the neuronal lineage rather than the glial lineage (Figure 2). This was an unexpected finding as BT 241, a glioblastoma, is a glial tumour thus would be expected to have more glial differentiation than neuronal (Bonavia *et al*., 2011; Holland, 2000;

Chen *et al*., 2011; Wen & Kesari, 2008). However, because BT 241 is a long term culture, it is possible that the clone which is selected for over multiple passages may be more prone to a neuronal phenotype. This selection phenomenon has been observed in some GBM cell lines which indicated a predominantly GFAP negative phenotype (Pollard *et al*., 2009). The current results still indicate some GFAP expression confirming that the selected subclone is a bipotential clone which has the ability to differentiate into multiple lineages. This result further shows the limitations of using cell lines and long term cultures as they select for particular clones which thrive in culture conditions.

BT 241 was subjected to all stem cell assays including the secondary sphere formation assay. This assay is used to determine the stem cell frequency within a population of cells through the analysis of secondary sphere formation which correlates with self-renewal capacity (Singh *et al*.,2004; Tropepe *et al*., 1999). When compared to three primary glioblastoma samples, BT 241 secondary sphere formation did appear higher but did not appear to be extremely different indicating that this primary sample showed an increased capacity for self-renewal but perhaps not significantly increased as the standard deviation for BT 241 overlapped with two out of three primary GBMs analysed (Figure 3).

Proliferation analysis of BT 241 revealed that cell proliferation increased over time as expected (Figure 5). BT 241 cells appeared to increase from day 0 to day 10 under both neural stem cell conditions and serum conditions. No significant differences in proliferation profile were found between culture conditions ($p>0.05$, Figure 5).

BT 241 was subjected to knockdown of Bmi1 using the lentiviral construct shBmi1 ***1*** and shLuc as a control. These lentiviral constructs had previously been validated both at the mRNA and protein levels (Figures 7 & 8). Once transduced, BT 241 cells were subjected to flow analysis. Flow analysis revealed an observed decrease of Bmi1 at the protein level supporting the previous finding that protein levels had been affected by the shBmi1 ***1*** construct (Figure 9). Interestingly, when BT 241 shLuc and shBmi1 ***1*** cells were analysed for the brain tumour initiating cell marker CD133, it was observed that knockdown of Bmi1 appeared to result in an increase in CD133 expression levels (Figure 9). This result is in keeping with previous unpublished findings within the Singh lab which suggest that Bmi1 epigenetically silences CD133. Previous findings indicate that when Bmi1 is knocked down, CD133 transcript levels increase. ChIP analysis at the CD133 promoter for the epigenetic activation mark 3meH3K4 as well as the epigenetic inhibition mark 3meH3K27 also revealed that when Bmi1 is knocked down, the activation mark 3meH3K4 is increased and the inhibition mark 3meH3K27 is decreased (unpublished data). Expression of the neural stem cell marker CD15 did not differ significantly between shLuc cells and shBmi1 ***1*** cells (Figure 9). This result is in keeping with other reports which indicate that CD15 expression remains stable in long term serum-free cultures and only decreases under differentiation conditions (Mao *et al*., 2009).

Bmi1 knockdown cells (shBmi1 ***1***) and control cells were analysed for self-renewal capacity using the secondary sphere formation assay. Bmi1 knockdown was found to have a significant effect on self-renewal when compared to control cells ($p=0.0004$, Figure 10). As well as significantly decreasing self-renewal, sphere size, a measure of proliferation (Tropepe *et al*., 1999), was affected by Bmi1 knockdown as seen by significantly smaller shBmi1 spheres as compared to shLuc spheres ($p=0.0058$, Figure 11). Proliferation of BT 241 shBmi1 ***1*** and shLuc

cells was also analysed using the CyQuant proliferation assay and revealed that Bmi1 knockdown cells exhibited significantly decreased proliferation when compared to control cells ($p<0.001$, Figure 12). These results are in keeping with previous findings indicating that Bmi1 knockdown has a negative effect on cell self-renewal and proliferation (Fasano *et al*., 2009; Molofsky *et al*., 2003; Bruggeman *et al*., 2007; Iwama *et al*., 2004; Schuringa & Vellenga, 2010; Abdouh *et al*., 2009; Chen *et al*., 2010; Gil *et al*., 2005; Lessard & Sauvageau, 2003). The proliferation results suggest that the loss of Bmi1 contributed to increased senescence and apoptosis, possibly as a result of decreased inhibition on p14 and p16 which affects the Rb and p53 tumour suppressor pathways. It has been shown that when Bmi1 is knocked down in stem cells, levels of p14arf and p16ink4a become upregulated and reactive oxygen species levels increase resulting in decreased cell growth and increased apoptosis (Bruggeman *et al*., 2005; Jacobs *et al*., 1999a; Lessard & Sauvageau, 2003; Liu *et al*., 2006; Molofsky *et al*., 2005; Schuringa & Vellenga, 2010; Zencak *et al*., 2005).

BT 241 shLuc and shBmi1 ***1*** cells were subjected to differentiation and analysed based on the markers MAP2, a marker of mature neurons, and GFAP, a marker of mature astrocytes. Immunofluorescence staining of differentiated cells was inconclusive as a result of potential non-specific binding of the GFAP antibody (Figure 14). Flow cytometric analysis of differentiation markers indicated higher overall neuronal differentiation than glial differentiation, consistent with previous BT 241 differentiation analysis (Figure 2). Neuronal differentiation appeared greater in Bmi1 knockdown cells as compared to control cells (Figure 15). This result was expected based on previous findings indicating that knockdown of Bmi1 results in increased differentiation (Abdouh *et al*., 2009; Ailles & Weissman, 2007; Bracken *et al*., 2006; Bruggeman *et al*., 2007; Chen *et al*., 2010; Fasano *et al*., 2007; Gil *et al*., 2005; Lessard & Sauvageau, 2003;

Park *et al*., 2004). Interestingly, glial differentiation appeared decreased in Bmi1 knockdown cells compared to control cells (Figure 15). This result was unexpected but may be the result of low cell number analysed and no technical replicates (Supplementary Figure 4).

To validate the use of BT 241 as a "spontaneous" GBM cell line, knockdown of Bmi1 using the lentiviral construct shBmi1 ***1*** and shLuc was performed in the commercial GBM cell line U-118 MG and cells were subjected to the same stem cell assays as BT 241. Knockdown of Bmi1 was validated at the mRNA level (Figure 16).

U-118 MG transduced cells were analysed for self-renewal capacity using the secondary sphere formation assay. In keeping with BT 241 findings, Bmi1 knockdown in U-118 MG cells was found to have a significant effect on self-renewal when compared to control cells ($p=0.0023$, Figure 17). Sphere size was also significantly decreased in U-118 MG Bmi1 knockdown cells compared to control cells ($p=0.0016$, Figure 18), similar to what was found in BT 241 cells.

Proliferation of U-118 MG shLuc and shBmi1 ***1*** cells was analysed using the CyQuant proliferation assay and revealed that Bmi1 knockdown cells exhibited significantly decreased proliferation when compared to control cells ($p<0.001$, Figure 19). These results confirm what was observed in BT 241 knockdown cells and are in keeping with previous findings indicating that Bmi1 knockdown has a negative effect on cell self-renewal and proliferation (Fasano *et al*., 2009; Molofsky *et al*., 2003; Bruggeman *et al*., 2007; Iwama *et al*., 2004; Schuringa & Vellenga, 2010; Abdouh *et al*., 2009; Chen *et al*., 2010; Gil *et al*., 2005; Lessard & Sauvageau, 2003).

U-118 MG shLuc and shBmi1 ***1*** cells were subjected to differentiation and analysed based on the markers MAP2 and GFAP to examine neuronal and glial differentiation, respectively.

Immunofluorescence staining of differentiated cells was inconclusive as a result of poor MAP2 staining and potential non-specific binding of the GFAP antibody as well as unhealthy cells (Figures 20 & 21). Flow cytometric analysis of differentiation markers indicated higher overall glial differentiation than neuronal differentiation (Figure 22). This finding opposed the results seen in BT 241 knockdown cells which indicated greater neuronal differentiation (Figure 15). This result is, however, in keeping with the morphology of glioblastoma tumours which arise from glial cells and show greater astrocytic differentiation (Bonavia *et al*., 2011; Holland, 2000; Chen *et al*., 2011; Wen & Kesari, 2008). Overall differentiation of cells appeared greater in Bmi1 knockdown cells as compared to control cells (Figure 22). This result was expected based on previous findings indicating that knockdown of Bmi1 results in increased differentiation (Abdouh *et al*., 2009; Ailles & Weissman, 2007; Bracken *et al*., 2006; Bruggeman *et al*., 2007; Chen *et al*., 2010; Fasano *et al*., 2007; Gil *et al*., 2005; Lessard & Sauvageau, 2003; Park *et al*., 2004). The differences found between BT 241 and U-118 MG differentiation profiles further indicate the limitations of using cell lines and long term cultures for experimental analysis as they select for particular clones which thrive in culture conditions over long periods of time.

To confirm knockdown of Bmi1 and to confirm that the functional results seen using shBmi1 ***1*** were a result of the construct targeting Bmi1 mRNA and not a result of off-target effects, three shRNAs targeting different areas of Bmi1 mRNA and a scrambled control (shControl) were used against BT 241 cells and transduced cells were subjected to stem cell assays. We compared all new constructs to our previously validated shLuc construct as well as untransduced U-118 MG GBM cells and found that all shBmi1 constructs appeared to knockdown Bmi1 (Figures 23 & 24). To our surprise, the scrambled control showed levels of Bmi1 similar to knockdown levels

and we therefore doubted it as a true control. Out of interest, we used previously acquired BT 241 shLuc data as an additional comparative control for subsequent results.

Secondary sphere formation for BT 241 transduced with shBmi1 ***2-4*** was analysed against both the scrambled control and shLuc. An extremely significant decrease in secondary sphere formation was found for all shBmi1 cells as well as the scrambled control when compared to shLuc (Figure 25). These results indicated that all shBmi1 constructs had a negative effect on self-renewal in BT 241 cells. No significant difference in average sphere size was observed for any shBmi1 used (Figure 26) however, these results are unreliable since the scrambled control was found to be affecting Bmi1 levels. Proliferation assays performed on BT 241 shBmi1 ***2-4*** and shControl cells revealed no significant difference in proliferative capacity between Bmi1 knockdown cells and control cells (Figures 27 & 28). This may be the result of the use of the scrambled control which was demonstrated as yielding Bmi1 levels comparable to all knockdown constructs. The potentially confounding control resulted in the proliferation assay being inconclusive, however, as this assay is time sensitive, no comparison to shLuc cells could be made to confirm these results.

BT 241 shBmi1 ***2-4*** and shControl cells were subjected to differentiation and analysed for MAP2 and GFAP expression levels by flow cytometry (Figure 30). No differences in expression level were observed between shControl and shBmi1 ***2-4*** for any of the markers examined (Figure 30). The differentiation profile of shBmi1 ***2-4*** and shControl cells indicated greater neuronal differentiation, as seen by higher MAP2 expression, and relatively low astrocytic differentiation, as seen by low GFAP expression (Figure 30). This result was consistent with the shLuc differentiation profile which indicated greater neuronal differentiation than glial differentiation (Figure 30). Interestingly, neuronal differentiation appeared dramatically decreased in shLuc

cells compared to all other transduced cells (Figure 30). This difference may merely be the result of one-time analysis of cells and low BT 241 cell number analysed (Supplementary Figure 4), however, this assumption would need to be confirmed by repeating the analysis.

In vivo analysis of Bmi1 knockdown was performed using BT 241 and the shBmi1 ***1*** and shLuc lentiviral constructs. Tumour formation was found in one NSG mouse injected with as low as 100 sorted BT 241 shLuc cells while no tumour formation was found in the corresponding NSG mouse injected with 100 sorted BT 241 shBmi1 cells (Figure 31). However, tumours were not found in NSG mice injected with 100 enriched cells. This inconsistency may be due to engraftment differences resulting from the injection of low cell numbers. It may be possible that some mice injected with 100 enriched cells did not receive all 100 cells as a result of technical limitations of manual injection of cells. It was observed that at lower cell numbers, Bmi1 knockdown appears to prevent tumour formation while control cells allow tumour formation to occur. Although tumours were found in mice injected with 10,000 and 50,000 BT 241 shBmi1***1*** cells, it was observed that tumours formed from shBmi1 ***1*** transduced cells showed mild to moderate infiltration by pleomorphic cells while shLuc transduced cells showed large tumour masses and increased infiltration (Figure 32). This observation suggests that Bmi1 knockdown had an effect on proliferation of tumour cells *in vivo*, resulting in smaller and less invasive tumours. To determine whether tumour size was affected by Bmi1 knockdown, a relative surface area for tumours was measured for both shLuc and shBmi1 ***1*** tumours at 10,000 and 50,000 cells. Tumour size appeared decreased in shBmi1 ***1*** tumours at both cell numbers with tumour size ranging from 0.2679 mm^2 to 5.3325 mm^2 as compared to control cells which had tumour sizes ranging from 5.621 mm^2 to 18.03 mm^2 (Table 1). The decrease in shBmi1 ***1*** tumours compared

to control tumours at 10,000 cells was not found to be statistically significant (Figure 33). This finding may have been the result of so few replicates used. The decrease in shBmi1***1*** tumour size as compared to shLuc tumours at 50,000 cells was not statistically analysed as there were not sufficient replicates (Figure 33). Although the results seen were not statistically significant, a trend indicating that tumours formed from Bmi1 knockdown cells were smaller than control tumours was observed. This result is in keeping with previous findings in Daoy medulloblastoma xenografts which displayed a decrease in tumour infiltration upon Bmi1 knockdown (Wang *et al*., 2011). Our current *in vivo* data suggests that at lower cell numbers, rate of tumour formation is affected by Bmi1 knockdown while at higher numbers, the size and invasiveness of tumour formation is affected by Bmi1 knockdown.

Tumour formation was seen in the NSG mouse injected with 23,000 sorted shBmi1 cells but not in control mice (Table 1). This observation may have been a result of cellular health and survival. For this set of injections, only 23,000 sorted cells were viable for injection. As the cells did not appear very healthy, tumour formation of shLuc cells may not have been possible as a result of poor cell survival upon injection. This potential issue is further supported by our observation that with 5000 cells or more, all mice injected with shLuc cells consistently show tumour formation (Table 1).

Pathologically, all tumours were described as highly pleomorphic, with vascular endothelial hypertrophy, high mitotic index and of epithelial origin. This is consistent with the primary patient glioblastoma tumour suggesting that the tumours formed recapitulated the primary patient tumour.

In conclusion, we find that Bmi1 knockdown has significant effects on self-renewal and proliferation in both a primary glioblastoma cell line, BT 241, and a commercially available glioblastoma cell line, U-118 MG. When Bmi1 is knocked down in these cells, we see marked decreases in self-renewal ability and proliferation over time. *In vivo*, we observe that at low cell numbers, Bmi1 knockdown appears to prevent tumour formation while at high cell numbers, Bmi1 knockdown appears to result in a decreased tumour size and invasiveness. Our observations both *in vitro* and *in vivo* suggest that Bmi1 may serve as a potential therapeutic target in glioblastoma tumours.

This study determined a significant role of Bmi1 in self-renewal and proliferation of cancer stem cells and found that Bmi1 is necessary for these stem cell functions. Future work should expand upon these findings to further determine the *in vivo* role of Bmi1 knockdown through increased animal injections. Future studies should also examine whether Bmi1 is sufficient to cause cancerous mutations and induce tumour initiation. Bmi1 overexpression studies in normal neural stem cells should be performed to determine whether Bmi1 mutations are sufficient to induce transformation of normal neural stem cells into cancer stem cells.

Chapter 5.

REFERENCES

Abdouh M, Facchino S, Chatoo W, Balasingam V, Ferreira J, Bernier G. (2009) **BMI1 Sustains Human Glioblastoma Multiforme Stem Cell Renewal**. *The Journal of Neuroscience*. **29**(28):8884-8896.

Ailles LE & Weissman IL. (2007) **Cancer stem cells in solid tumors**. *Current Opinions in Biotechnology*. **18**:460-466.

Al-Hajj M, Wicha MS, Benito-Hernandez A, Morrison SJ, Clarke MF. (2003) **Prospective identification of tumorigenic breast cancer cells**. *PNAS*. **100**(7):3983-3988.

Alkema MJ, Wiegant J, Raap AK, Berns A, van Lohiuzen M. (1993) **Characterization and chromosomal localization of the human proto-oncogene BMI-1**. *Human Molecular Genetics*. **2**(10):1597-1603.

Bao S, Wu Q, McLendon RE, Hao Y, Shi Q, Hjelmeland AB, Dewhirst MW, Bigner DD, Rich JN. (2006) **Glioma stem cells promote radioresistance by preferential activation of the DNA damage response**. *Nature*. **444**:756-760.

Bracken AP, Dietrich N, Pasini D, Hansen KH, Helin K. (2006) **Genome-wide mapping of Polycomb target genes unravels their roles in cell fate transitions**. *Genes & Development*. **20**:1123-1136.

Bracken AP, Kleine-Kohlbrecher D, Dietrich N, Pasini D, Gargiulo G, Beekman C, Theilgaard-Monch K, Minucci S, Porse BT, Marine JC, Hansen KH, Helin K. (2007) **The Polycomb group proteins bind throughout the INK4A-ARF locus and are disassociated in senescent cells**. *Genes & Development*. **21**:525-530.

Bonavia R, Inda M, Cavenee WK, Furnari FB. (2011) **Heterogeneity Maintenance in Glioblastoma: A Social Network**. *Cancer Research*. **71**(12):1-6.

Bonnet D & Dick JE. (1997) **Human acute myeloid leukemia is organized as a hierarchy that originates from a primitive hematopoietic cell**. *Nature Medicine*. **3**(7):730-737.

Bruggeman SW, Hulsman D, Tanger E, Buckle T, Blom M, Zevenhoven J, van Tellingen O, van Lohuizen M. (2007) **Bmi1 controls tumor development in an Ink4a/Arf-independent manner in a mouse model for glioma**. *Cancer Cell*. **12**(4):328-41.

Bruggeman SW, Hulsman D, van Lohuizen M. (2009) **Bmi1 deficient neural stem cells have increased Integrin dependent adhesion to self-secreted matrix**. *Biochimica et Biophysica Acta*. **1790**(5):351-360.

Bruggeman SW, Valk-Lingbeek ME, van der Stoop PP, Jacobs JJL, Keiboom K, Tanger E, Hulsman D, Leung C, Arsenijevic Y, Marino S, van Lohuizen M. (2005) **Ink4a and Arf differentially affect cell proliferation and neural stem cell self-renewal in Bmi1-deficient mice**. *Genes & Development*.**19**(12):1438-43.

Chen H, Zhou L, Dou T, Wan G, Tang H, Tian J. (2011) **BMI1's maintenance of the proliferative capacity of laryngeal cancer stem cells**. *HEAD & NECK*. **33**(8):1115-1125.

Chen R, Nishimura MC, Bumbaca SM, Kharbanda S, Forrest WF, Kasman IM, Greve JM, Soriano RH, Gilmour LL, Rivers CS, Modrusan Z, Nacu S, Guerrero S, Edgar KA, Wallin JJ, Lamszus K, Westphal M, Heim S, James CD, VandenBerg SR, Costello JF, Moorefield S, Cowdrey CJ, Prados M, Phillips HS. (2010) **A Hierarchy of Self-Renewing Tumor-Initiating Cell Types in Glioblastoma**. *Cancer Cell*. **17**:362-375.

Chiba T, Miyagi S, Saraya A, Aoki R, Seki A, Morita Y, Yonemistsu Y, Yokosuka O, Taniguchi H, Nakauchi H, Iwama A. (2008) **The Polycomb Gene Product BMI1 Contributes to the Maintenance of Tumor-Initiating Side Population Cells in Hepatocellular Carcinoma**. *Cancer Research*. **68**(19):7742-7749.

Clarke MF, Dick JE, Dirks PB, Eaves CJ, Jamieson CHM, Jones DL, Visvader J, Weissman IL, Wahl GM. (2006) **Cancer Stem Cells – Perspectives on Current Status and Future Directions: AACR Workshop on Cancer Stem Cells**. *Cancer Research*. **66**(19):9339-9344.

Cohen KJ, Hanna JS, Prescott JE, Dang CV. (1996) **Transformation by the Bmi-1 Oncoprotein Correlates with Its Subnuclear Localization but Not Its Transcriptional Suppression Activity**. *Molecular and Cellular Biology*. **16**(10):5527-5535.

Corti S, Locatelli F, Papadimitriou D, Donadoni C, Salani S, Del Bo R, Strazzer S, Bresolin N, Comi GP. (2006) **Identification of a Primitive Brain-Derived Neural Stem Cell Population Based on Aldehyde Dehydrogenase Activity**. *Stem Cells*. **24**:975-985.

Dalerba P, Cho RW, Clarke MF. (2007) **Cancer Stem Cells: Models and Concepts**. *Annual Review of Medicine*. **58**:267-284.

Dimri GP, Martinez JL, Jacobs JJL, Keblusek P, Itahana K, van Lohuizen M, Campisi J, Wazer DE, Band V. (2002) **The Bmi-1 Oncogene Induces Telomerase Activity and Immortalizes Human Mammary Epithelial Cells**. *Cancer Research*. **62**:4736-4745.

Emmenegger BA & Wechsler-Reya RJ. (2008) **Stem Cells and the Origin and Propagation of Brain Tumors**. *Journal of Child Neurology*. **23**:1172-1178.

Fan C, He L, Kapoor A, Rybak AP, De Melo J, Cutz JC, Tang D. (2009) **PTEN inhibits BMI1 function independently of its phosphatise activity**. *Molecular Cancer*. **8**:98-112.

Fasano CA, Dimos JT, Ivanova NB, Lowry N, Lemischka IR, Temple S. (2007) **shRNA Knockdown of Bmi-1 Reveals a Critical Role for p21-Rb Pathway in NSC Self-Renewal during Development**. *Cell Stem Cell*. **1**:87-99.

Galli R, Binda E, Orfanelli U, Cipelletti B, Gritti A, De Vitis S, Fiocco R, Foroni C, Dimeco F, Vescovi A. (2004) **Isolation and Characterization of Tumorigenic, Stem-like Neural Precursors from Human Glioblastoma**. *Cancer Research*. **64**:7011-7021.

Gil J, Bernard D, Peters G. (2005) **Role of Polycomb Group Proteins in Stem Cell Self-Renewal and Cancer**. *DNA and Cell Biology*. **24**(2):117-125.

Ginestier C, Hur MH, Charafe-Jauffret E, Monville F, Dutcher J, Brown M, Jacquemier J, Viens P, Kleer CG, Liu S, Schott A, Hayes D, Birnbaum D, Wicha MS, Dontu G. (2007) **ALDH1 Is a Marker of Normal and Malignant Human Mammary Stem Cells and a Predictor of Poor Clinical Outcome**. *Cell Stem Cell*. **1**:555-567.

Grinstein E & Wernet P. (2007) **Cellular signaling in normal and cancerous stem cells**. *Cellular Signalling*. **19**:2428-2433.

Hadjipanayis CG & Van Meir EG. (2009) **Tumor initiating cells in malignant gliomas: biology and implications for therapy**. *Journal of Molecular Medicine*. **87**:363-374.

Haupt Y, Alexander WS, Barri G, Klinken SP, Adams JM. (1991) **Novel Zinc Finger Gene Implicated as *myc* Collaborator by Retrovirally Accelerated Lymphomagenesis in Eμ-*myc* Transgenic Mice**. *Cell*. **65**:753-763.

He S, Iwashita T, Buchstaller J, Molofsky AV, Thomas D, Morrison SJ. (2009) **Bmi-1 over-expression in neural stem/progenitor cells increases proliferation and neurogenesis in culture but has little effect on these functions in vivo**. *Developmental Biology*. **328**:257-272.

Hess DA, Meyerrose TE, Wirthlin L, Craft TP, Herrbrich PE, Creer MH, Nolta JA. (2004) **Functional characterization of highly purified human hematopoietic repopulating cells isolated according to aldehyde dehydrogenase activity**. *Blood*. **104**:1648-1655.

Holland EC. (2000) **Glioblastoma multiforme: The terminator**. *PNAS*. **97**(12):6242-6244.

Huse JT & Holland EC. (2010) **Targeting brain cancer: advances in the molecular pathology of malignant glioma and medulloblastoma**. *Nature Reviews*. **10**:319-331.

Ishizawa K, Rasheed ZA, Karisch R, Wang Q, Kowalski J, Susky E, Pereira K, Karamboulas C, Mogal N, Rajeshkumar NV, Hidalgo M, Tsao M, Ailles L, Waddell TK, Maitra A, Neel BG, Matsui W. (2010) **Tumor-Initiating Cells Are Rare in Many Human Tumors**. *Cell Stem Cell*. **7**:279-282.

Ivanchuk SM, Mondal S, Dirks PB, Rutka, JT. (2001) **The *INK4A/ARF* locus: Role in cell cycle control and apoptosis and implications for glioma growth**. *Journal of Neuro-Oncology*. **51**: 219-229.

Iwama A, Oguro H, Negishi M, Kato Y, Morita Y, Tsukui H, Ema H, Kamijo T, Katoh-Fukui T, Koseki H, van Lohuizen M, Nakauchi H. (2004). **Enhanced Self-Renewal of Hematopoietic Stem Cells Mediated by the Polycomb Gene Product Bmi-1**. *Immunity*. **21**: 843-851.

Jacobs JJL, Kieboom K, Marino S, DePinho RA, van Lohuizen M. (1999a). **The oncogene and Polycomb-group gene bmi-1 regulates cell proliferation and senescence through the ink4a locus**. *Nature*. **397**:164-168.

Jacobs JJL, Scheijen B, Voncken JW, Kieboom K, Berns A, van Lohuizen M. (1999b). **Bmi-1 collaborates with c-Myc in tumorigenesis by inhibiting c-Myc-induced apoptosis via INK4a/ARF**. *Genes & Development*. **13**:2678-2690.

Jiang L, Li J, Song L. (2009) **Bmi-1, stem cells and cancer**. *Acta Biochimica et Biophysica Sinica*. 1-8.

Kallin EM, Cao R, Jothi R, Xia K, Cui K, Zhao K, Zhang Y. (2009) **Genome-Wide uH2A Localization Analysis Highlights Bmi1-Dependent Deposition of the Mark at Repressed Genes**. *PLoS Genetics*. **5**(6):e1000506. doi:10.1371/journal.pgen.1000506.

Kelly PN, Dakic A, Adams JM, Nutt SL, Strasser A. (2007) **Tumor Growth Need Not Be Driven by Rare Cancer Stem Cells**. *Science*. **317**:337.

Kim JH, Yoon SY, Kim CN, Joo JH, Moon SK, Choe IS, Choe YK, Kim JW. (2004) **The Bmi-1 oncoprotein is overexpressed in human colorectal cancer and correlates with the reduced p16INK4a/p14ARF proteins**. *Cancer Letters*. **203**:217-224.

Lessard J & Sauvageau G. (2003). **Bmi-1 determines the proliferative capacity of normal and leukaemic stem cells**. *Nature.* **423**(6937):255-60.

Li Z, Cao R, Wang M, Myers MP, Zhang Y, Xu RM. (2006). **Structure of a Bmi-1-Ring1B Polycomb Group Ubiquitin Ligase Complex**. *Journal of Biological Chemistry*. **281**(29):20643-20649.

Li Z, Wang H, Eyler CE, Hjelmeland AB, Rich JN. (2009). **Turning Cancer Stem Cells Inside Out: An Exploration of Glioma Stem Cell Signaling Pathways**. *The Journal of Biological Chemistry.* **284**(25):16705-16709.

Liu L, Andrews LG, Tollefbol, TO. (2006) **Loss of the human polycomb group protein BMI1 promotes cancer-specific cell death**. *Oncogene*. **25**: 4370-4375.

Mao X, Zhang X, Xue X, Guo G, Wang P, Zhang W, Fei Z, Zhen H, You S, Yang H. (2009) **Brain Tumor Stem-Like Cells Identified by Neural Stem Cell Marker CD15**. *Translational Oncology*. **2**(4):247-257.

Marquardt JU, Factor VM, Thorgeirsson SS. (2010) **Epigenetic regulation of cancer stem cells in liver cancer: Current concepts and clinical implications**. *Journal of Hepatology*. **53**:568-577.

Miller CR & Perry A. (2007) **Glioblastoma: Morphologic and Molecular Genetic Diversity**. *Archives of Pathology & Laboratory Medicine*. **131**(3):397-406.

Molofsky AV, Pardal R, Iwashita T, Park IK, Clarke MF, Morrison SJ. (2003) **Bmi-1 dependence distinguishes neural stem cell self-renewal from progenitor proliferation**. *Nature*. **425**(6961): 962-967.

Molofsky AV, He S, Bydon M, Morrison SJ, Pardal R. (2005) **Bmi-1 promotes neural stem cell self-renewal and neural development but not mouse growth and survival by repressing the p16Ink4a and p19Arf senescence pathways**. *Genes & Development*. **19**(12):1432-7.

O'Brien CA, Kreso A, Dick JE. (2009) **Cancer Stem Cells in Solid Tumors: An Overview**. *Seminars in Radiation Oncology*. **19**:71-77.

Oliver TG & Wechsler-Reya RJ. (2004) **Getting at the Root and Stem of Brain Tumors**. *Neuron*. **42**:885-888.

Pardal R, Clarke MF, Morrison SJ. (2003) **Applying the principles of stem-cell biology to cancer**. *Nature Reviews Cancer*. **3**:895-902.

Park IK, Morrison SJ, Clarke MF. (2004) **Bmi1, stem cells, and senescence regulation**. *Journal of Clinical Investigation*. **113**:175-179.

Pollard SM, Yoshikawa K, Clarke ID, Danovi D, Stricker S, Russell R, Bayani J, Head R, Lee M, Bernstein M, Squire JA, Smith A, Dirks P. (2009) **Glioma Stem Cell Lines Expanded in Adherent Culture Have Tumor-Specific Phenotypes and Are Suitable for Chemical and Genetic Screens**. *Cell Stem Cell*. **4**:568-580.

Qian T, Lee J-Y, Park J-H, Kim H-J, Kong G. (2010) **Id1 enhances RING1b E3 ubiquitin ligase activity through the Mel-18/Bmi1 polycomb group complex**. *Oncogene*. **29**:5818-5827.

Rahman M. (2009) **Introduction to Flow Cytometry**. Oxford: MorphoSys UK Ltd.

Reya T, Morrison SJ, Clarke MF, Weissman IL. (2001) **Stem cells, cancer, and cancer stem cells**. *Nature*. **414**:105-111.

Rosen JM & Jordan CT. (2009) **The Increasing Complexity of the Cancer Stem Cell Paradigm**. *Science*. **324**:1670-1673.

Sauvageau M & Sauvageau G. (2010) **Polycomb Group Proteins: Multi-Faceted Regulators of Somatic Stem Cells and Cancer**. *Cell Stem Cell*. **7**:299-313.

Schuringa JJ & Vellenga E. (2010) **Role of the polycomb group gene BMI1 in normal and leukemic hematopoietic stem and progenitor cells**. *Current Opinion in Hematology*. **17**: 294-299.

Shackleton M, Quintana E, Fearon ER, Morrison SJ. (2009) **Heterogeneity in Cancer: Cancer Stem Cells versus Clonal Evolution**. *Cell*. **138**:822-829.

Sharpless NE & DePinho RA. (1999) **The INK2A/ARF locus and its two gene products**. *Current Opinions in Genetics & Development*. **9**:22-30.

Shipitsin M & Polyak K. (2008) **The cancer stem cell hypothesis: in search of definitions, markers, and relevance**. *Laboratory Investigation*. **88**:459-463.

Silva J, Garcia JM, Pena C, Garcia V, Dominguez G, Suarez D, Camacho FI, Espinosa R, Provencio M, Espana P, Bonilla F. (2006) **Implication of Polycomb Members Bmi-1, Mel-18, and Hpc-2 in the Regulation of p16INK4a, p14ARF, h-TERT, and c-MYC Expression in Primary Breast Carcinomas**. *Clinical Cancer Research*. **12**(23):6929-6936.

Singh SK, Clarke ID, Terasaki M, Bonn VE, Hawkins C, Squire J, Dirks PB. (2003) **Identification of a Cancer Stem Cell in Human Brain Tumors**. *Cancer Research*. **63**:5821-5828.

Singh SK, Clarke ID, Hide T, Dirks PB. (2004a) **Cancer stem cells in nervous system tumors**. *Oncogene*. **23**:7267-7273.

Singh SK, Hawkins C, Clarke ID, Squire JA, Bayani J, Hide T, Henkelman RM, Cusimano MD, Dirks PB. (2004b) **Identification of human brain tumor initiating cells**. *Nature*. **432**(7015):396-401.

Steinbach D, Legrand O. (2007) **ABC transporters and drug resistance in leukemia: was P-gp nothing but the first head of the hydra?**. *Leukemia*. **21**:1172-1176.

Tabatabai G & Weller M. (2011) **Glioblastoma stem cells**. *Cell Tissue Research*. **343**:459-465.

Tan BT, Park CY, Ailles LE, Weissman IL. (2006) **The cancer stem cell hypothesis: a work in progress**. *Laboratory Investigation*. **86**:1203-1207.

Tropepe V, Sibilia M, Ciruna BG, Rossant J, Wagner EF, van der Kooy D. (1999) **Distinct neural stem cells proliferate in response to EGF and FGF in the developing mouse telencephalon.** *Developmental Biology*. **208**(1):166-88.

Uchida N, Buck DW, He D, Reitsma MJ, Masek M, Phan TV, Tsukamoto AS, Gage FH, Weissman IL. (2000) **Direct isolation of human central nervous system stem cells**. *PNAS*. **97**(26):14720-14725.

Valk-Lingbeek ME, Bruggeman SW, van Lohuizen M. (2004) **Stem Cells and Cancer: The Polycomb Connection**. *Cell*. **118**:409-418.

van Lohuizen M, Verbeek S, Scheijen B, Wientjens E, van der Gulden H, Berns A. (1991) **Identification of Cooperating Oncogenes in Eμ-*myc* Transgenic Mice by Provirus Tagging**. *Cell*. **65**:737-752.

Verhaak RGW, Hoadley KA, Purdom E, Wang V, Qi Y, Wilkerson MD, Miller CR, Ding L, Golub T, Mesirov JP, Alexe G, Lawrence M, O'Kelly M, Tamayo P, Weir BA, Gabriel S, Winckler W, Gupta S, Jakkula L, Feiler HS, Hodgson JG, James CD, Sarkaria JN, Brennan C, Kahn A, Spellman PT, Wilson RK, Speed TP, Gray JW, Meyerson M, Getz G, Perou CM, Hayes DN. (2010) **Integrated Genomic Analysis Identifies Clinically Relevant Subtypes of Glioblastoma Characterized by Abnormalities in *PDGFRA, IDH1, EGFR,* and *NF1***. *Cancer Cell*. **17**(1):98-110.

Vescovi AL, Galli R, Reynolds BA. (2006) **Brain tumour stem cells**. *Nature Reviews*. **6**:425-436.

Visvader JE & Lindeman GL. (2008) **Cancer stem cells in solid tumours: accumulating evidence and unresolved questions**. *Nature Reviews*. **8**:755-768.

Voncken JW, Schweizer D, Aagaard L, Sattler L, Jantsch MF, van Lohuizen M. (1999) **Chromatin-association of the Polycomb group protein BMI1 is cell cycle-regulated and correlates with its phosphorylation status**. *Journal of Cell Science*. **112**: 4627-4639.

Wang H, Wang L, Erdjument-Bromage H, Vidal M, Tempst P, Jones RS, Zhang Y. (2004) **Role of histone H2A ubiquitination in Polycomb silencing**. *Nature*. **431**:873-878.

Wang X, Venugopal C, Manoranjan B, McFarlane N, O'Farrell E, Nolte S, Gunnarsson T, Hollenberg R, Kwiecien J, Northcott P, Taylor MD, Hawkins C, Singh SK. (2011) **Sonic hedgehog regulates Bmi1 in human medulloblastoma brain tumor-initiating cells**. *Oncogene.* 1-13. doi: 10.1038/onc.2011.232.

Wen PY, Kesari S. (2008) **Malignant Gliomas in Adults**. *New England Journal of Medicine*. **359**:492-507.

Wicha MS, Liu S, Dontu G. (2006) **Cancer Stem Cells: An Old Idea – A Paradigm Shift**. *Cancer Research*. **66**(4):1883-1890.

Yadirgi G, Leinster VHL, Acquati S, Bhagat H, Shakhova O, Marino S. (2011) **Conditional Activation of Bmi1 Expression Regulates Self-Renewal, Apoptosis and Differentiation of Neural Stem/Progenitor Cells In Vitro and In Vivo**. *Stem Cells*. **29**(4):700-712.

Yin AH, Miraglia S, Zanjani ED, Almeida-Porada G, Ogawa M, Leary AG, Olweus J, Kearney J, Buck DW. (1997) **AC133, a Novel Marker for Human Hematopoietic Stem and Progenitor Cells**. *Blood*. **90**(12):5002-5012.

Zencak D, Lingbeek M, Kostic C, Tekaya M, Tanger E, Hornfeld D, Jaquet M, Munier FL, Schorderet DF, van Lohuizen M, Arsenijevic, Y. (2005) **Bmi1 Loss Produces an Increase in Astroglial Cells and a Decrease in Neural Stem Cell Population and Proliferation**. *The Journal of Neuroscience*. **25**(24):5774-5783.

SUPPLEMENTARY MATERIALS

Supplementary Table 1

Antigen	Antibody	Company	Catalogue No.	Dilution
CD133	PE	M. Bio	130-090-853	1:20
	PE Isotype	M. Bio	130-092-215	1:20
Bmi1	APC	R&D Systems	IC33341A	1:100
	APC Isotype	R&D Systems	130-092-217	1:100
MAP2	AlexaFluor 647	BD Biosciences	560382	1:10 (Flow cytometry) 1:20 (Immunofluorescence)
	Alexa 647 Isotype	Invitrogen	06013427	1:10 (Flow cytometry) 1:20 (Immunofluorescence)
GFAP (conjugated)	PE	BD Biosciences	561483	1:20
	PE Isotype	M. Bio	130-092-215	1:20
GFAP (unconjugated)	Rabbit, polyclonal	Dako	Z0334	1:2000
Rabbit IgG	Goat, Alexa-Fluor 647 conjugated	Invitrogen	A21245	1:1000

Supplementary Figure 1

Genecopoeia vectors

Japan vector

RING finger binding domain

Supplementary Figure 2

A) BT 241 under NSC conditions stained for CD133

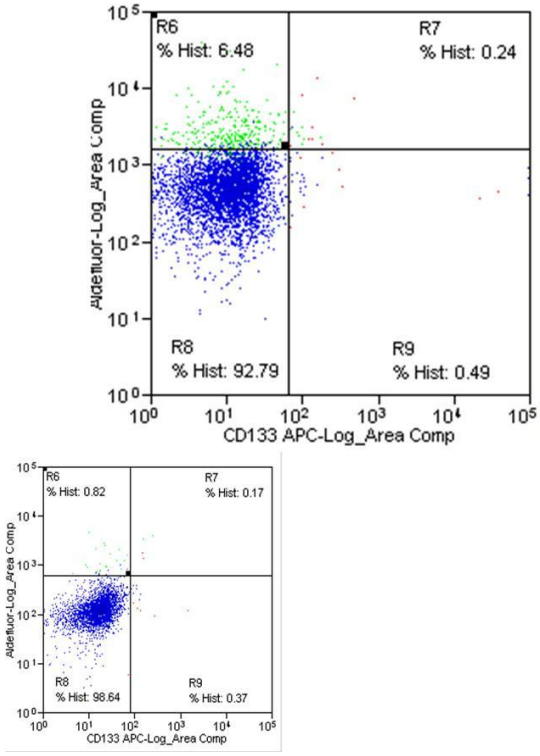

B) BT 241 under NSC conditions stained for Bmi1, MAP2, and GFAP

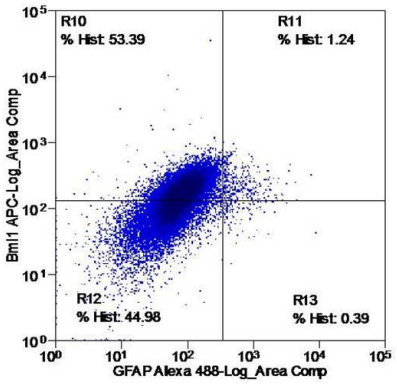

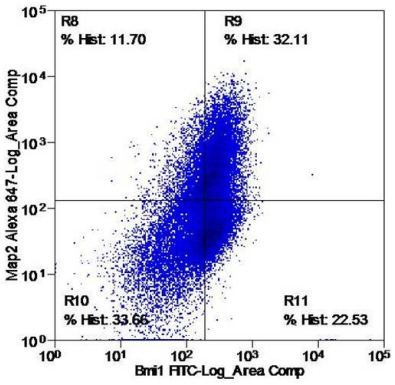

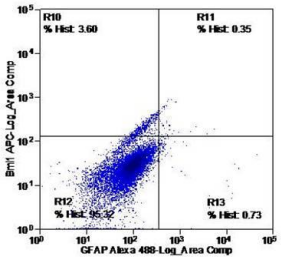

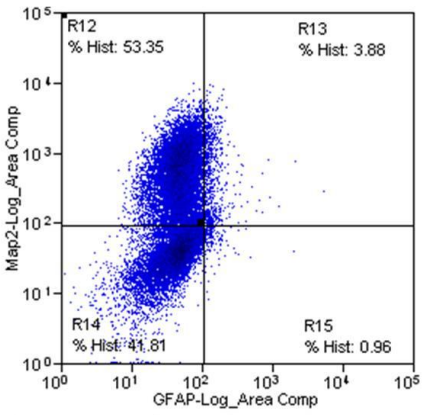

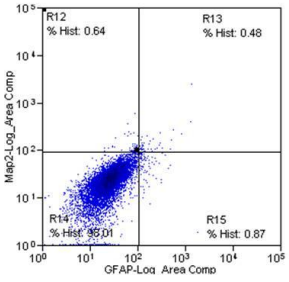

C) BT 241 under Differentiation conditions stained for CD133

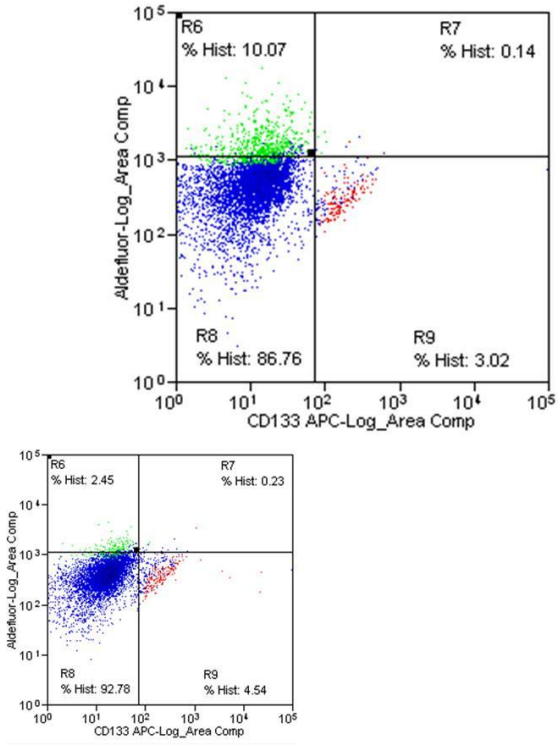

D) BT 241 under Differentiation conditions stained for Bmi1, MAP2, and GFAP

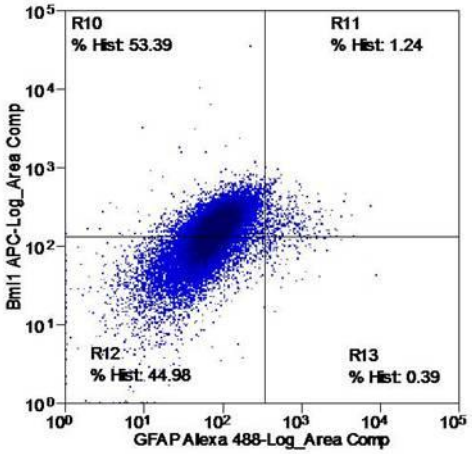

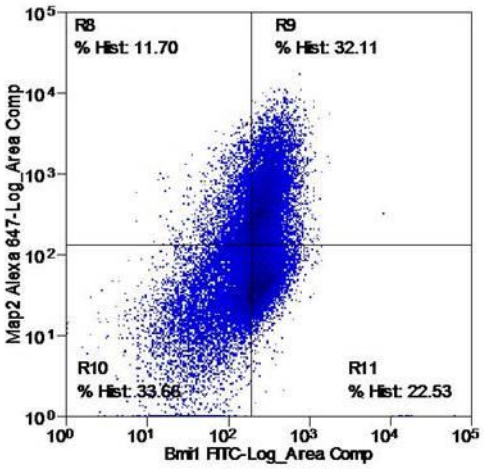

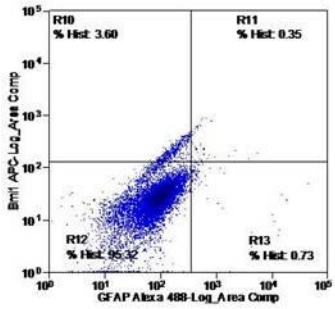

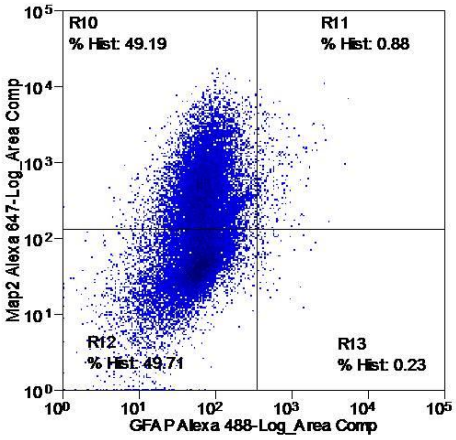

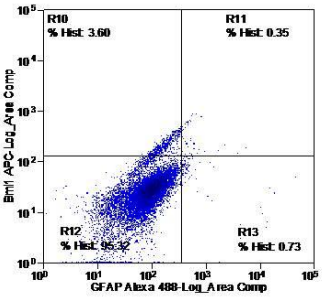

Supplementary Figure 3

A) Scatter plots for BT 241 shLuc cells stained for Bmi1, CD133, and CD15

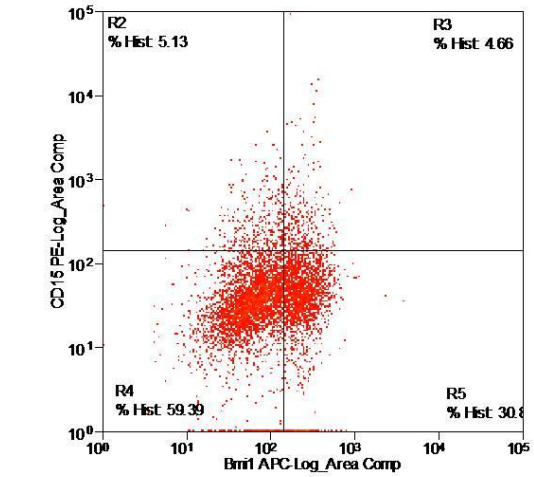

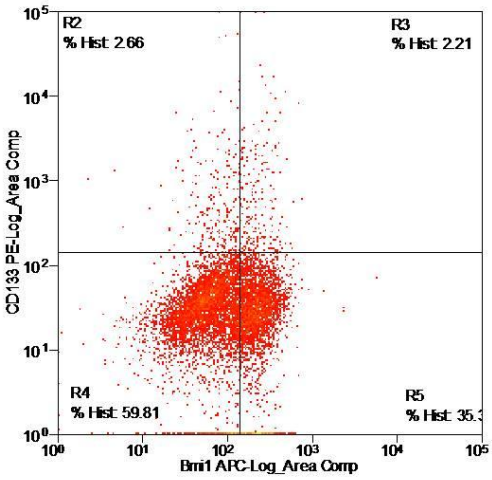

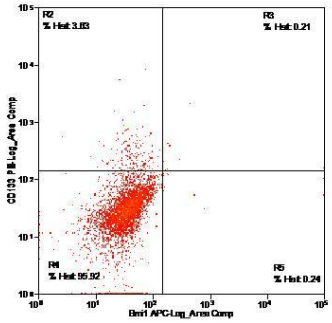

B) Scatter plots for BT 241 shBmi1 *1* cells stained for Bmi1, CD133, and CD15

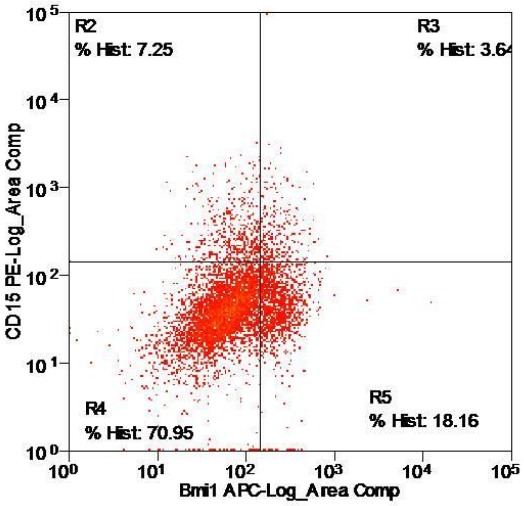

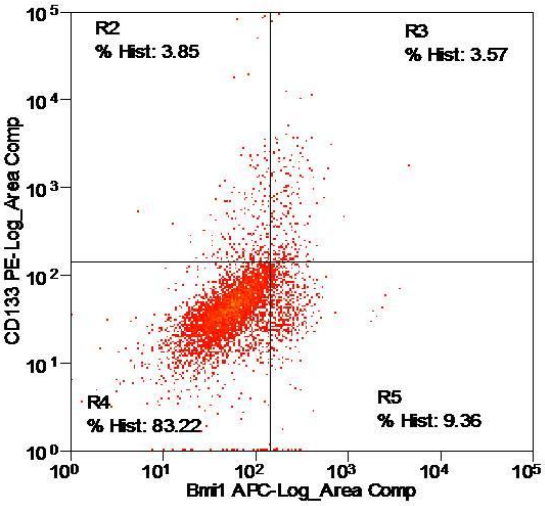

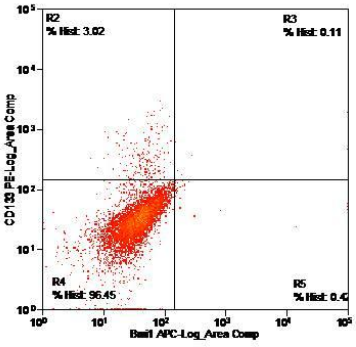

Supplementary Figure 4

A) BT 241 shLuc Differentiation

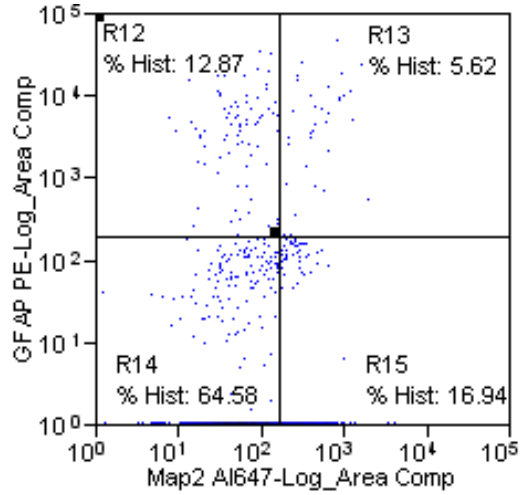

B) BT 241 shBmi1 Differentiation

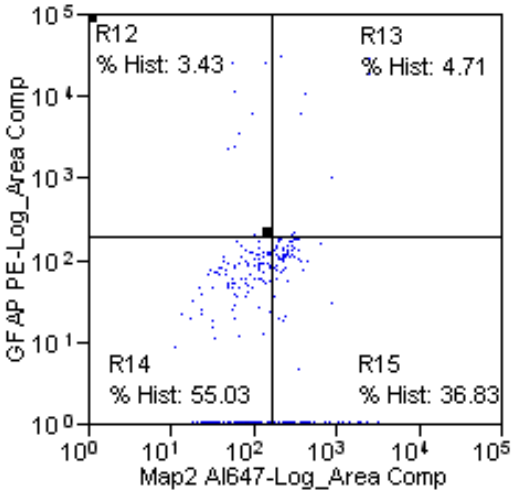

Supplementary Figure 5

A) U-118 MG shLuc Differentiation

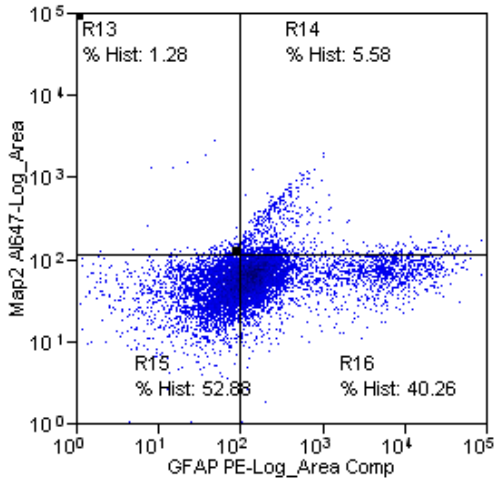

B) U-118 MG shBmi1 Differentiation

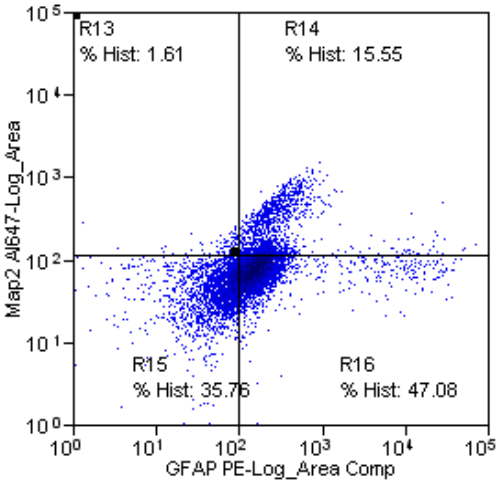

Supplementary Figure 6

A) Flow cytometric analysis of GFP expression in BT 241 shControl cells

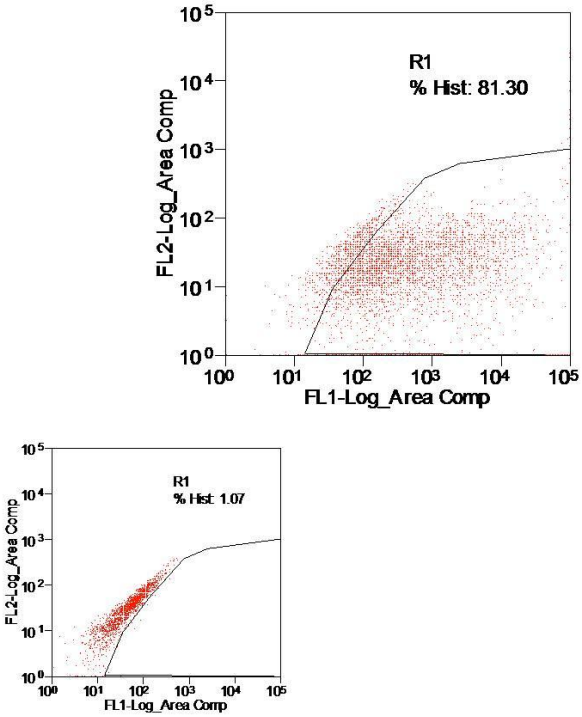

B) Flow cytometric analysis of GFP expression in BT 241 shBmi1 *2* cells

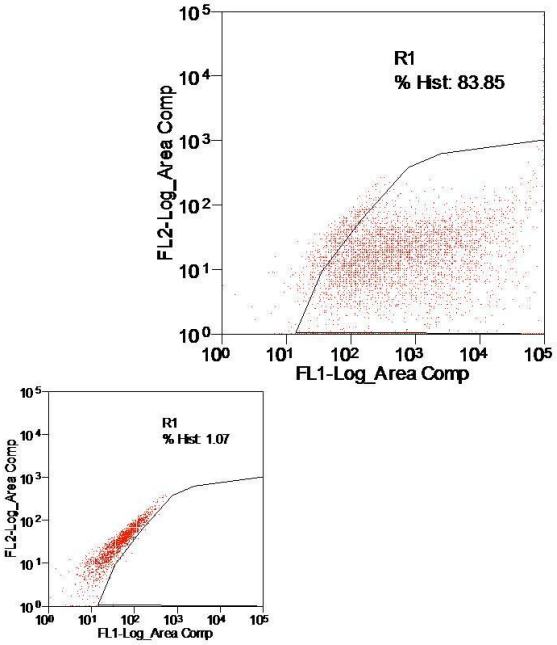

C) Flow cytometric analysis of GFP expression in BT 241 shBmi1 *3* cells

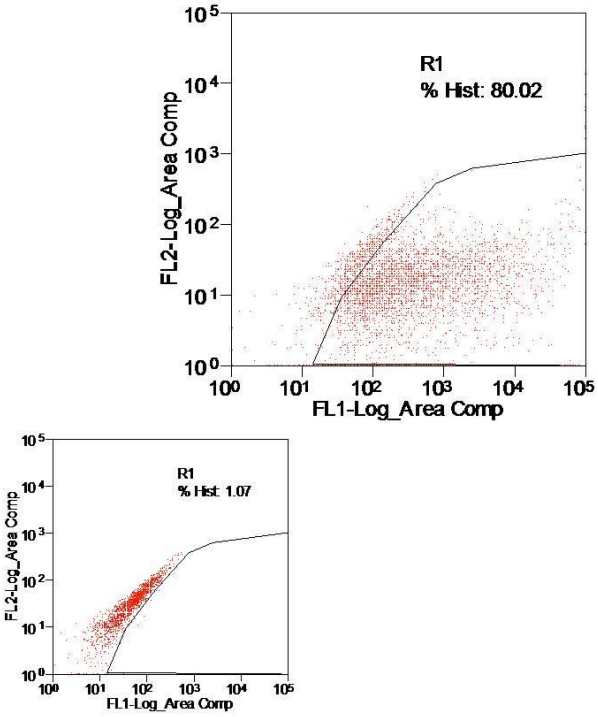

D) Flow cytometric analysis of GFP expression in BT 241 shBmi1 *4* cells

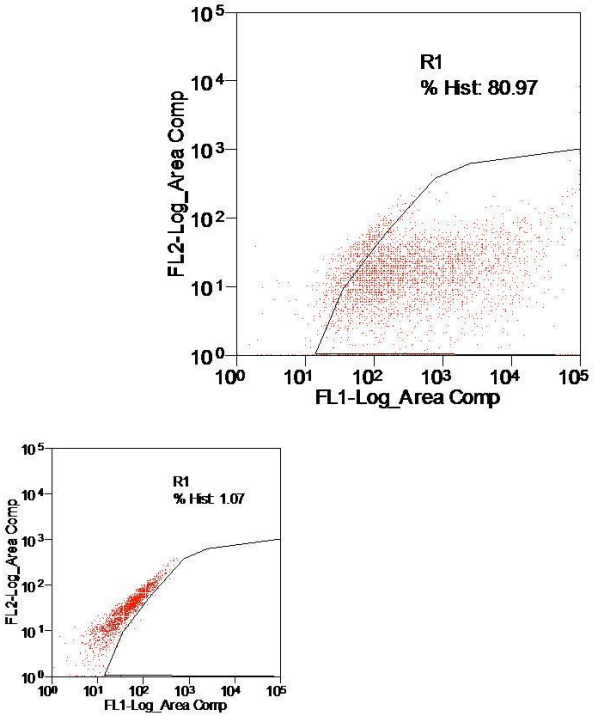

Supplementary Figure 7

A) Flow cytometric analysis of differentiation marker expression in BT 241 shControl cells

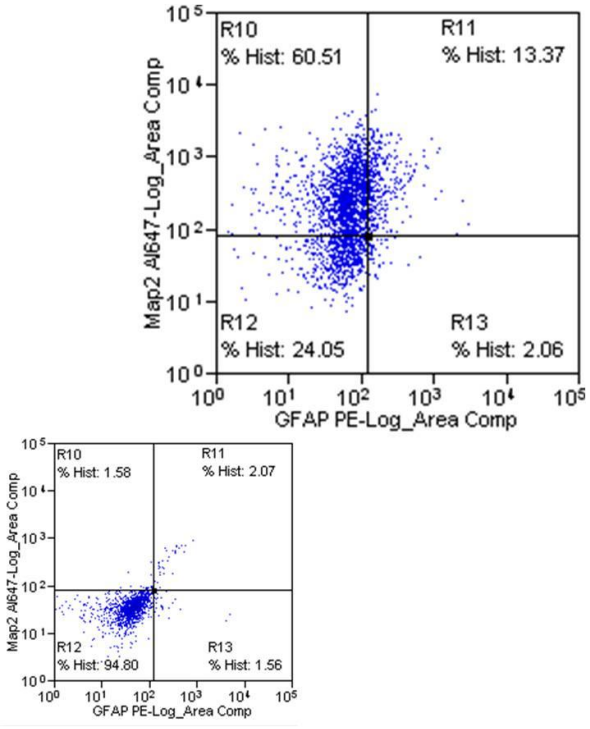

B) Flow cytometric analysis of differentiation marker expression in BT 241 shBmi1 *2* cells

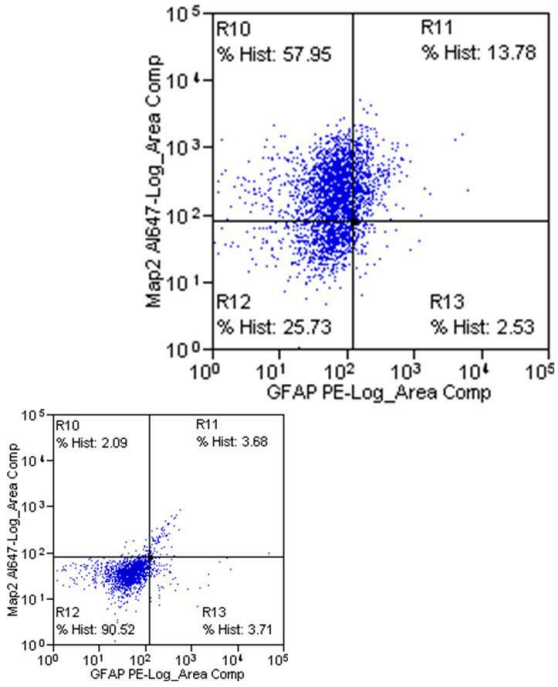

C) Flow cytometric analysis of differentiation marker expression in BT 241 shBmi1 *3* cells

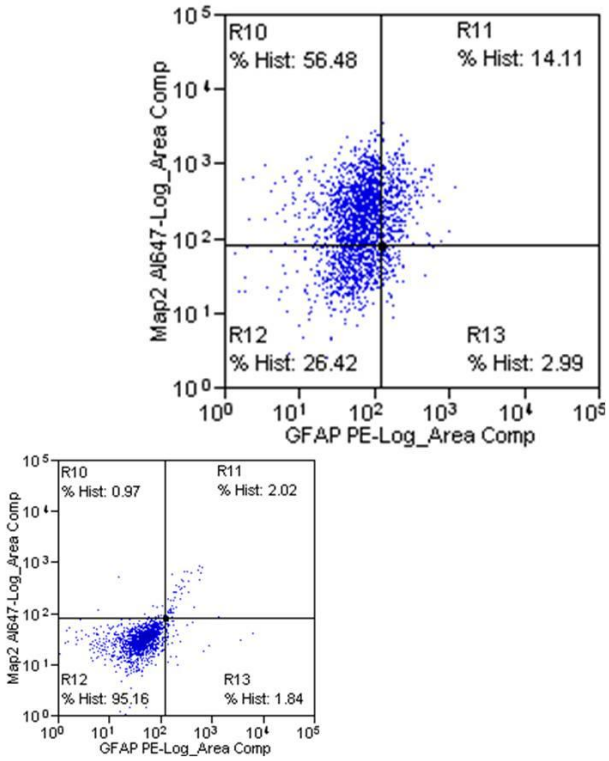

D) Flow cytometric analysis of differentiation marker expression in BT 241 shBmi1 *4* cells